RESEARCH ARTICLE

THE FASEB JOURNAL

The Journal of the Federation of American Societies for Experimental Biology

Longitudinal peripheral tissue RNA-Seq transcriptomic profiling, hyperalgesia, and wound healing in the rat plantar surgical incision model

Taichi Goto[1] | Matthew R. Sapio[2] | Dragan Maric[3] | Jeffrey M. Robinson[4] | Anthony F. Domenichiello[5] | Leorey N. Saligan[1] | Andrew J. Mannes[2] | Michael J. Iadarola[2]

[1]Symptoms Biology Unit, National Institute of Nursing Research, National Institutes of Health, Bethesda, MD, USA

[2]Department of Perioperative Medicine, Clinical Center, National Institutes of Health, Bethesda, MD, USA

[3]Flow and Imaging Cytometry Core Facility, National Institute of Neurological Disorders and Stroke, National Institutes of Health, Bethesda, MD, USA

[4]Translational Life Science Technology Program, University of Maryland, Baltimore County, Baltimore, MD, USA

[5]Lipid Peroxidation Unit, Laboratory of Clinical Investigation, National Institute on Aging, National Institutes of Health, Baltimore, MD, USA

Correspondence
Michael J. Iadarola, Department of Perioperative Medicine, Clinical Center, Building 10, Room 3D56, 10 Center Drive, MSC 1510, National Institutes of Health, Bethesda, MD 20892-1510, USA.
Email: michael.iadarola@nih.gov

Abstract

Postoperative pain and delayed healing in surgical wounds, which require complex management strategies have understudied complicated mechanisms. Here we investigated temporal changes in behavior, tissue structure, and transcriptomic profiles in a rat model of a surgical incision, using hyperalgesic behavioral tests, histological analyses, and next-generation RNA sequencing, respectively. The most rapidly (1 hour) expressed genes were the chemokines, *Cxcl1* and *Cxcl2*. Consequently, infiltrating leukocytes were abundantly observed starting at 6 and peaking at 24 hours after incising which was supported by histological analysis and appearance of the neutrophil markers, *S100a8* and *S100a9*. At this time, hyperalgesia was at a peak and overall transcriptional activity was most highly activated. At the 1-day timepoint, *Nppb*, coding for natriuretic peptide precursor B, was the most strongly upregulated gene and was localized by in situ hybridization to the epidermal keratinocytes at the margins of the incision. *Nppb* was basically unaffected in a peripheral inflammation model transcriptomic dataset. At the late phase of wound healing, five secreted, incision-specific peptidases, *Mmp2*, *Aebp1*, *Mmp23*, *Adamts7*, and *Adamtsl1*, showed increased expression, supporting the idea of a sustained tissue remodeling process. Transcripts that are specifically upregulated at each timepoint in the incision model may be potential candidates for either biomarkers or therapeutic targets for wound pain and wound healing. This study incorporates the examination of longitudinal temporal molecular responses, corresponding anatomical localization, and hyperalgesic behavioral alterations in the surgical incision model that together provide important and novel foundational knowledge to understand mechanisms of wound pain and wound healing.

KEYWORDS
cytokines, macrophage, neutrophil, postoperative pain, wound healing

1 | INTRODUCTION

Approximately 11% of Medicare beneficiaries have at least one type of wound, costing the US $28.1 to 96.8 billion, annually.[1] Postoperative pain and impaired healing in surgical wounds have major clinical consequences. Up to 85% of postoperative patients experience wound pain and of those, 75% report moderate to extreme pain during the immediate postoperative period.[2] Currently, many non-opioid approaches to perioperative pain are being implemented to avoid the use of opiates; despite these innovations, control of pain in the postoperative period remains strongly reliant on opioids,[3-5] which could lead to the development of tolerance, addiction, and diversion. To improve patient outcomes and reduce medical costs, it is critical to understand the etiology of pain and the healing process in surgical wounds to properly assess and adequately manage surgical wounds, postoperative pain, and potentially to accelerate repair and resolution of tissue injury.

Understanding the complex factors and mechanisms that commonly influence wound pain and wound healing processes is an essential step in the identification of clinically useful biomarkers of wound pain and wound healing. The evolving temporal stages of wound healing reflect different biological mechanisms comprising multiple molecular and intercellular communication networks. For example, pro-inflammatory cytokines, growth factors, and various hormones have been associated with wound pain, which have also informed the wound-healing progress.[6,7] However, a variety of factors, including the environment and stress, which are sometimes uncontrollable, can affect wound status.[8,9] These complexities make understanding the full biological dynamics of wounds challenging, and make predicting which path a wound will take, to healing or chronification, difficult to determine.

To address fundamental molecular aspects of wound response and repair, we performed a fine-grained temporal analysis of gene regulatory programs that occur in rat hind paw following surgical incision.[10] From the standpoint of incisional pain, previous studies have conducted transcriptome analysis utilizing the rat incision model in dorsal spinal cord[11] and dorsal root ganglia.[12] The present report addresses the peripheral input components driving modulation of primary afferent and second-order spinal neuronal responses. To explore gene regulation related to pain initiation, maintenance, and resolution in conjunction with tissue repair (wound healing), we applied next-generation RNA sequencing analysis to the local incised tissue. Our analysis involved longitudinal transcriptomic and anatomical analyses from 0 hour (untreated control) to 12 days after incising. In the longitudinal dataset we determined subcellular locations of induced gene products,

examined transcripts related to wound healing, and compared the incision results to a transcriptomic dataset from a peripheral inflammation model induced by hind paw carrageenan injection, a widely used model for investigating acute inflammatory processes and neuronal hyperalgesia.[13-15] Comparing the dynamic evolution of gene profiles from the two pathophysiological states revealed surgical incision-specific gene regulatory programs coinciding with the time course of hyperalgesia and allodynia, patterns of local cellular activation and leukocyte infiltration, and processes governing wound resolution. Many of the factors identified represent new, or reinforce known, pathways for the study of inflammation, nociceptive pain, and tissue repair. The results provide potential leads for the development of biomarkers for wound pain and wound healing and may extend to new methods of treatment.

2 | MATERIALS AND METHODS

2.1 | Animal care, surgical incision model, and peripheral inflammation model

Experiments were approved by the Institutional Animal Care and Use Committee of the Clinical Center, National Institutes of Health (Bethesda, Maryland). Animals were cared for and tested in accordance with ethical guidelines established in the NIH Guide for Care and Use of Laboratory Animals. Male Sprague-Dawley rats (200 to 300 g) were housed in pairs with 12-hours light-dark cycles, had access to food and water ad libitum, and were tested and monitored for behavior during the animal's light cycle. Animal cages were furnished with a plastic tunnel for enrichment.

A surgical incision on the plantar aspect of the rat hind paw was made as previously described.[10,11] Briefly, a 1-cm longitudinal incision was made through the skin and fascia with a sterile no. 15 scalpel blade, and the incision was extended into the underlying plantar flexor digitorum brevis muscle with a no. 11 scalpel blade. The wound was closed with two horizontal mattress sutures by 5-0 nylon suture (Johnson & Johnson, New Brunswick, New Jersey). Animals were sacrificed before incising and at 1 and 6 hours, and 1, 3, 6, and 12 days after incising. Hind paw tissues were harvested for next-generation RNA sequencing and histological and in situ hybridization analyses. We used five to six rats for hind paw thickness measurement, behavioral testing, RNA extraction, and histology for each timepoint.

Acute inflammation was induced in the male Sprague Dawley rats by injection of freshly prepared 4% (W/V) of carrageenan in 0.9% sterile saline into the left hind paw. Rats were sacrificed before the injection as well as at 1, 4, 8, 24, 48, and 72 hours after the injection, and hind paw

tissues were harvested for next-generation RNA sequencing and histological and in situ hybridization analyses. In the inflammation group, we used three to six rats for hind paw thickness measurement and behavioral test, and three rats for RNA extraction and histology for each timepoint. Part of the data obtained from these rats were used in our previous study.[16]

2.2 | Hind paw edema evaluation and behavioral tests

Hind paw edema was evaluated by measuring hind paw thickness using a caliper. Values are indicated as mean with SEM. The hind paw thickness was analyzed using two-way ANOVA with Sidak's post-hoc multiple comparison method.

Thermal hyperalgesia was detected by the Plantar Test Instrument (Ugo Basile, Comerio, Italy). Unrestrained rats were placed on a glass platform under a plastic enclosure for at least seven minutes for habituation. Then, an infrared laser was applied to generate thermal stimuli, and the time until paw withdrawal occurred was recorded, or the thermal stimulus was terminated at 25 seconds if no withdrawal occurred. Mechanical allodynia was detected by calibrated von Frey monofilaments. For the incision model, animals were placed on an elevated wire mesh surface, and von Frey filaments producing a bending force of 0.4 g, 1 g, 2 g, 4 g, or 6 g were applied near the distal edge of the wound for 1 to 3 seconds. Filaments were tested 10 times in the order of increasing force, and the number of brisk paw withdrawals was counted.[11,17] For the inflammation model, animals were placed on an elevated wire mesh surface, and monofilaments of increasing bending force were applied to the plantar surface of hind paws until two consecutive withdrawals for a particular filament were observed or 60 g (the cutoff value) was reached. Then monofilaments of decreasing strength were applied until consecutive withdrawals were not observed. The up-down method was continued until the thresholds became consistent. If no withdrawal response was observed, the cutoff value 60 g was recorded. Values are indicated as mean with SEM. The results of behavioral tests were analyzed using repeated-measures two-way ANOVA with Sidak's post-hoc multiple comparison method.

2.3 | RNA purification, library preparation, and next-generation sequencing

Rat plantar tissue was dissected and frozen at –80°C. Total RNA was extracted following the protocol from the

RNeasy Tissue Mini Kit including the optional DNase digestion (Qiagen, USA). Briefly, tissue was homogenized in TRIzol (Life Technologies, Carlsbad, CA) using the FastPrep-24 Homogenizer (MP Biomedicals, Solon, OH). Chloroform was added, and the aqueous layer was extracted. An equal volume of 70% ethanol was added, and the RNA was bound to the spin column. The column was washed and then incubated with RNase-Free DNase (Qiagen) at room temperature for 15 minutes. The columns were washed again, and RNA was eluted off the column in RNase-free water. RNA integrity was evaluated using a 2100 Bioanalyzer and the RNA 6000 Nano Kit (Agilent Technologies, Santa Clara, CA). All samples had an RNA integrity score greater than or equal to 8.3.

Sequencing libraries were constructed from 1 µg total RNA using TruSeq Stranded Total RNA Library Prep Globin (Cat. No. 20020612, Illumina, Inc) used according to the manufacturer's instructions. Adapters were IDT for Illumina - TruSeq RNA UD Indexes. Amplification was performed using 10 cycles which was optimized for the input amount and to minimize the chance of over-amplification. Libraries were pooled in equimolar amounts for sequencing. The pooled libraries were sequenced on a NovaSeq 6000 to achieve a minimum of 46 million 150 base read pairs. The data was processed using RTA version 3.3.3.

2.4 | Alignment and quantification of RNA-Seq count data

Alignment of the RNA-Seq datasets was performed using MAGIC software and a Rn6 genomic target with RefSeq annotations.[11,18] Gene quantification is reported as significant fragments per kilobase per million aligned reads (sFPKM). The calculation for sFPKM estimates the expression level from read counts to limit the influence of protocol biases as described previously.[19] Briefly, this measure corrects for several sources of distortion such as transcript length, GC content, library sequencing depth, genomic contamination, and insert size. Throughout the manuscript, we represent changes of gene expression in terms of expression ratio. In this calculation, we smooth the effects of dividing by very low sFPKM values by adding a small number (0.1) to both the numerator and denominator using the following formula:

$$\text{Expression ratio} = \frac{\text{sFPKM (each timepoint)} + 0.1}{\text{sFPKM (untreated control)} + 0.1}$$

We identified differentially expressed genes (DEGs) by comparing the distributions of gene expression of each gene across two sample groups of timepoints in both directions individually. This analysis was part of the MAGIC pipeline

and was performed using default parameters as described previously.[18] Briefly, a DEG score in the range of 0 to 200 was given to each gene, where 200 indicates a gene for which the expression values separate perfectly between the two groups examined. A threshold was chosen by setting the false discovery rate (FDR) to no more than 5%. As an additional consideration, in some cases the FDR is automatically selected lower than 5% in cases where the addition of more genes would exceed an incremental FDR of 20%. This occurs in situations when there are high confidence DEG populations with very low FDR calculations, where the addition of additional DEGs to reach an average value of 5% adds genes with low confidence estimates. Detailed statistical methods and validation of these techniques have been reported previously.[18,19]

2.5 | Hierarchical clustering and heatmap generation

To cluster genes based on their expression patterns, hierarchical clustering and heatmap visualizations were performed on sFPKM values. Before plotting in the heatmap, expression was transformed by dividing each value by the maximum sFPKM for that gene across the timepoints, resulting in values between 0 and 1. DEGs between any two timepoints were used to construct a heatmap based on ratios of expression between timepoints, representing the time course of gene expression over time. The heatmap data were clustered using the dist (Euclidean) and hclust (ward.d2) functions in R and plotted using heatmap·2 with viridis "inferno" coloration. The clustering analysis broke the gene expression patterns into 14 visually distinct groups. For heatmaps with smaller numbers of genes, expression was transformed by dividing each value by the maximum sFPKM for that gene across the timepoints, resulting in values between 0 and 1, and ratios are plotted for each gene relative to maximum expression. These heatmaps were created by Microsoft Excel for Mac 16.16.18 and sorted by peak expression in the time course, and then secondarily sorted by max sFPKM value. The yellow, white, and purple colors indicate 1, 0.5 and 0, respectively.

2.6 | Classification of subcellular compartment among DEGs

We assorted genes into five exclusive categories based on the major subcellular localization of the mature protein: secreted, extracellular proteins, plasma membrane, cytoplasm, and nucleus. Uncategorized/other genes are reported as a sixth category. The "secreted" designation is defined as proteins located outside of the cell membrane and the "extracellular proteins" label is defined as proteins

located in the extracellular space but part of a multicellular organism such as extracellular proteins. This classification was performed based on data from the following databases: Uniprot,[20] LocDB,[21] COMPARTMENTS,[22] and Human Protein Atlas (http://www.proteinatlas.org),[23] all of which are available publicly. Data on subcellular localization of all genes were extracted from each of these databases and examined. Due to the lack of a consistent labeling schema throughout these four databases, the information was manually harmonized using the literature to conform to the six categories reported in Figures 2A and 5B. A small number of genes did not match any of these databases and were also classified based on literature searching.

2.7 | Gene ontology analyses

Gene ontology (GO) analysis was performed to explore transcripts related to both wound healing and sensory perception of pain. Genes were annotated using the GO terms of "wound healing" which consists of 404 genes, and of "sensory perception of pain" which consists of 194 genes in the Rat Genome Database.[24]

2.8 | Immune cell and pathway analysis with the Imsig R package

The Imsig R package was used to estimate relative immune cell abundance at each timepoint. The Imsig tests for co-expression of several dozen cell-type specific (or primarily cell-type specific) genes to develop a relative score for immune cell type abundance and biological pathway activity including interferon, proliferation, and translation in the incised hind paw tissue. The Imsig paper and the software repositories (CRAN and GitHub) provide complete gene lists used for score determination, and further detail on how scores are calculated.[25] We have already applied the Imsig tests to a carrageenan-induced peripheral inflammation model.[16] The Imsig tests in the present study provides results consistent with canonical patterns of inflammatory and nociceptive induction/resolution in this rat surgical incision model. Implementation of the Imsig package in this study is described in a new GitHub repository (https://github.com/PhyloGrok/Analy zeComplexTissues), with the processed data and R-code used for this analysis provided open-source.

2.9 | Histological analyses

Animals were deeply anesthetized and perfused intracardially with cold phosphate-buffered saline followed by 4%

paraformaldehyde. Tissue was dissected and post-fixed in 4% paraformaldehyde for a minimum of 16 hours but not more than 36 hours. Samples were embedded in paraffin blocks, 6 μm sections were cut, mounted, and stained by Histoserv Inc (Germantown, MD). Hematoxylin-eosin and Masson's trichrome staining were performed to obtain standard assessments of, respectively, general histological and connective tissue parameters.

Multiplex in situ hybridization was conducted using the RNAscope Multiplex Fluorescent assays v2 (Advanced Cell Diagnostics, Newark, CA) with Tyramide Signal Amplification (Opal Reagent Systems; Perkin Elmer, Waltham MA) on the formalin fixed paraffin embedded sections. Stained sections were imaged using an Axio Imager.Z2 slide scanning fluorescence microscope (Zeiss, Oberkochen, Germany) equipped with a 20X/0.8 Plan-Apochromat (Phase-2) non-immersion objective (Zeiss), a high-resolution ORCA-Flash4.0 sCMOS digital camera (Hamamatsu, Shizuoka, Japan), a 200W X-Cite 200DC broad band lamp source (Excelitas Technologies, Waltham MA) and 5 customized filter sets (Semrock, Rochester NY) optimized to detect the following fluorophores: DAPI, Opal520, Opal570, Opal620, and Opal690. Image tiles (600 × 600 mm viewing area) were individually captured at 0.325 micron/pixel spatial resolution, and the tiles seamlessly stitched into whole specimen images using the ZEN 2 image acquisition and analysis software program (Zeiss), with an appropriate color table applied to each image channel to either match its emission spectrum or to set a distinguishing color balance. Pseudocolored stitched images were overlaid as individual layers to create multicolored merged composites.

The images were processed by Adobe Photoshop 20.0.0 and ImageJ 2.0.0-rc-69/1.52p to analyze co-localization of detected genes from the multiplex in situ hybridization images.

3 | RESULTS

From the surgical incision model, we detected 12 454 DEGs that were significantly up- or down- regulated in at least one of the observed timepoints compared with the baseline (untreated control) value of each gene. We excluded a total of 2140 uncharacterized genes from the dataset. The remaining 10 314 genes were analyzed further (Table S1). Gene level categorization related to general properties, such as highest alterations across the time course, or more specific categorization such as genes in the incisional secretome, or genes related to tissue repair often identify genes that span more than one classification criteria, and these are encountered in several of the heat maps.

3.1 | Surgical incision-induced inflammation and DEGs

Hind paw edema, thermal hyperalgesia, and mechanical allodynia were induced in the incised hind paw. Hind paw edema was present within 1 hour after incising and was sustained for 12 days (Figure 1A). Thermal hyperalgesia was also detected at the earliest time point tested (6 hours after incising) and sustained for at least 3 days (Figure 1B). Further, VFT testing detected significant mechanical allodynia (Figures 1C,D, and S1). The VFT using a 1 g hair indicated that the severest mechanical allodynia occurred at 1 day after incising (Figure 1C) and with the 4 g hair mechanical allodynia could be detected out to 3 days. Figure 1E shows macroscopic and microscopic images over the time course of the incised hind paw. Microscopically, the epidermal layer of the incision was closed by 1-3 days after incising, while incisional damage was still found in the dermal layer. Infiltrating leukocytes were abundantly observed from 1 to 12 days after incising as shown in high-power photomicrographs to the right of the hind paw images. Newly produced collagen tissue was clearly observed from 3 days after incising and replaced the dermal layer at 12 days (see also Figure 3A). The epidermal layer was thickened from 1 day after incising and this abnormal finding was sustained through 12 days. The panels of gene expression ratios in Figure 1F show an overview of the differentially induced and suppressed genes at each timepoint with several examples labeled. The peak number of induced genes occurred at 3 days after incising (4040 genes) and the peak of suppressed genes was at 1 day after incising (1938 genes) (Table 1). Hierarchical clustering and heatmap visualization were performed using 3500 genes that showed the highest expression ratio, which determined 14 gene clusters (Figure 1G). Figure 1H and Table 2 show the 50 genes with the highest induced expression following incision. Of the 50 genes, 42 genes had their peak expression between 6 hours and 1 day after incising. The most rapidly expressed genes were two chemokine coding genes, *Cxcl1* and *Cxcl2* (Figure 1H), which are known neutrophil chemoattractants.[26] While peak expression was observed 6 hours after incising, some interleukin encoding genes, *Il1b* and *Il6*, began to be upregulated as rapidly as 1 hour after incising. At this time, the anti-inflammatory cytokine, *Il10*, was also upregulated, and the induction, going from 0.2 to 6.0 sFPKM, provides a contrast to the much more robust induction occurring with *Cxcl1* and *Cxcl2* (0.9 to 468.4 and 0.2 to 105.3 sFPKM, respectively) (Figure 1F, see also Figure 2C,D).
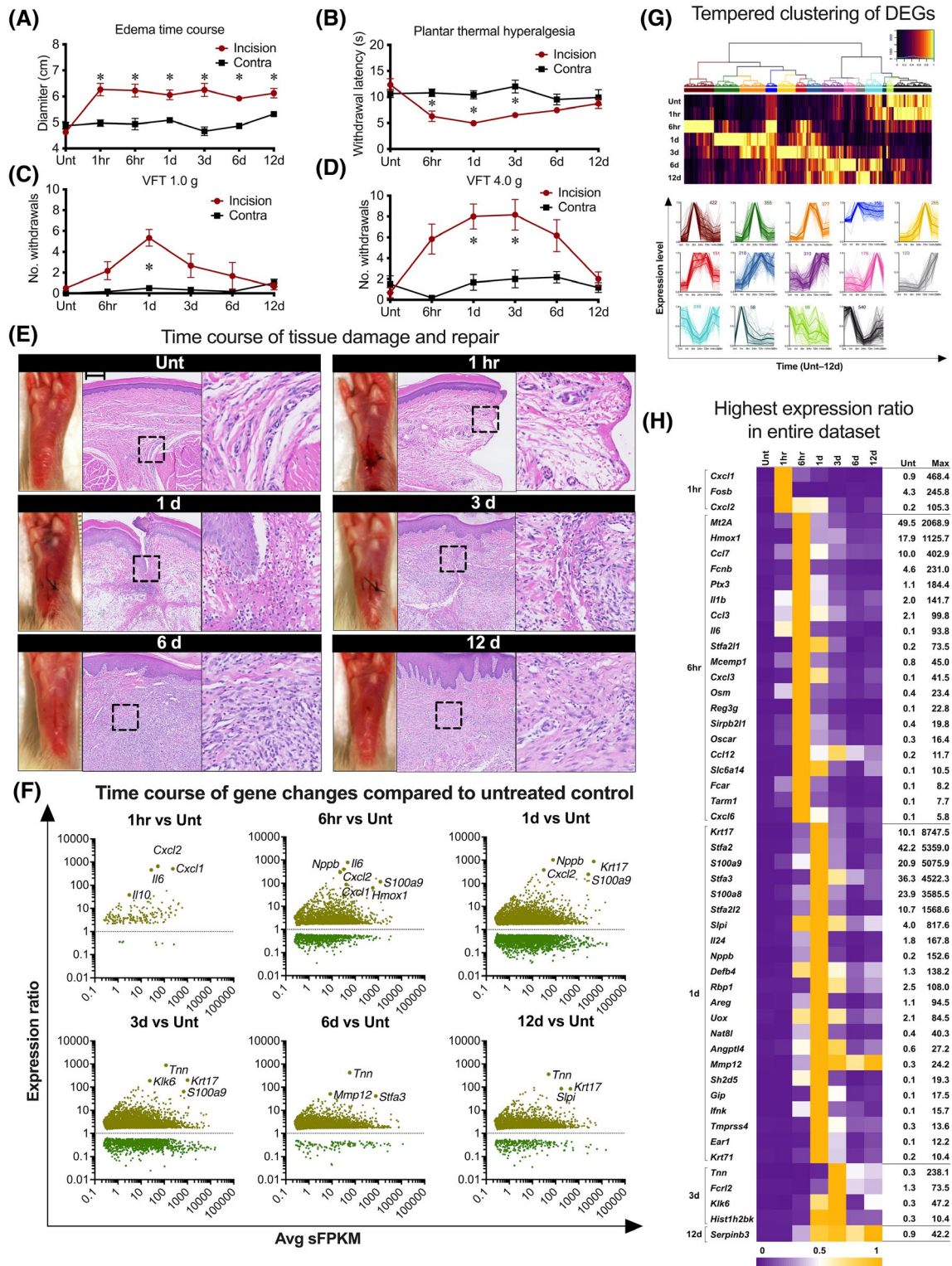
FIGURE 1　Hind paw inflammation and overview of differentially expressed genes at each timepoint. A, Edema measured by width of hind paws in the incision side and the untreated control side. B, The withdrawal latency to thermal stimulation in the incision side and the untreated control side. C, von Frey test using 1 g hair in the incision side and the untreated control side. D, von Frey test using 4 g hair in the incision side and the untreated control side. E, Photomicrographs of hematoxylin and eosin staining of incised hind paw tissues. Black bar in the middle panel of untreated control indicates 200 μm. Right side panels in each figure are high power images of the region indicated the black dashed boxes. F, Overview of differentially increased and decreased genes at each timepoint with several representative genes labeled. For the scatter plot, the expression ratio between each timepoint and untreated control is plotted versus average sFPKM using logarithmic scales. G, Gene clusters based on temporal patterns. H, The top 50 differentially expressed genes. avg, average; d, day(s); hr or h, hour(s); Unt, untreated control; VFT, von Frey test

TABLE 1 Number of differentially expressed genes at each timepoint

	1 hr	6 hr	1 d	3 d	6 d	12 d
Induced	177	2479	3832	4040	3446	2390
Suppressed	9	892	1938	1112	132	271

Abbreviations: d, day(s); hr, hours.

3.2 | Subcellular localizations and the incisional secretome

To further explore the cellular and biochemical characteristics of transcriptomic profiles in the incision model, we determined the subcellular location of each gene. Over time the number of DEGs gradually increased and reached a peak at 1 day after incising (Figure 2A left and Table 3). The proportion of genes encoding secreted proteins at 1 hour was twice as high as that at baseline (untreated control). The proportion of genes coding for secreted products decreased at 1 day and then underwent an increase of 84.8%-93.9% between 6-12 days. This complement of genes was distinct from the genes undergoing alterations at the earlier times. The proportion of genes whose protein product was located in the nucleus was increased by approximately 10 points (34%) compared with the untreated control at 1 day, while genes in other categories were unchanged or decreased (Figure 2A right and Table 3).

Key intercellular regulators of tissue and systemic biological responses to incision were examined by focusing on genes encoding secreted proteins and peptides. We refer to this set of transcripts as "the incisional secretome" and it consists of 442 genes (Figure 2B) in aggregate over the full 12-day time course. The incisional secretome comprised 4.3% of the genes in the total hind paw incision dataset of 10 314 genes examined (Table 3). Among the 389 genes for which the maximum sFPKM values were over 1.0, the range of expression ratios was 1.0 (eg *Sod3*, *Ecm1*, and *Nov*) to 1017.1 (*Nppb*). Overall, the greatest number of DEGs coding for secreted products was observed at 6 days after incising and the highest expression changes occurred at the 6-hour and 1-day timepoints (Figure 2B-D). Focusing on the 30 genes that had the highest expression ratio, the major classes in the incisional secretome were chemokines and interleukins such as *Cxcl1*, *Cxcl2*, *Il10*, *Ccl7*, *Il1b*, *Ccl3*, *Il6*, *Cxcl3*, *Ccl20*, *Ccl12*, *Ccl17*, *Cxcl6*, and *Il24*, which are known to have important roles in orchestrating inflammatory responses (Figure 2D and Table 4). In addition to cell signaling molecules, three matrix metalloproteases, *Mmp9*, *Mmp12*, and *Mmp13*, had their highest expression ratio at 1 day after incising. *Tnn* (tenascin N, integrin ligand regulating cellular recruitment and angiogenesis, 0.3 to 238.1 sFPKM) and *Lcn2* (lipocalin 2,

a 19 kDa lipid-binding protein, 2.6 to 94.8 sFPKM) were the two most strongly regulated transcripts at 3 days after incising.

3.3 | Transcripts related to wound-healing

We examined genes implicated in the wound healing process out to day 12 in the hind paw incision model. Masson's trichrome staining for connective tissue (collagen, stained blue) was used to track incisional healing (Figure 3A). From 6 hours after incising, a thickened epidermal layer was observed and was present through the remainder of the timepoints. The epidermal layer was almost closed by 1 day after incising, but the incisional damage was observed in deeper layers until 3 days after incising. Additionally, the dense collagen tissues in the dermal layer were still observed at the later timepoints through days 3 to 12. New collagen synthesis was clearly observed from 3 days after incising, and the damaged tissue was completely replaced by the newly synthesized collagen by 12 days after incising. Leukocyte infiltration commenced at 6 hours and an abundant accumulation was seen at 1 day after incising.

Among the DEGs, we detected 353 wound-healing–related genes. Their temporal changes are indicated in Figure 3B,C. The majority of genes that had peak expression between 6 hours and 1 day after incising were hardly expressed in the untreated control, which suggests that the appearance of many of these transcripts can be attributed to genes expressed by infiltrating leukocytes and/or were more specifically induced by the wound healing process than other genes. To obtain a more detailed transcriptomic assessment, we extracted the 30 wound-healing–related genes that had the highest expression ratio (Figure 3D and Table 5) and to focus on potential, accessible biomarker candidates, we also extracted those that encode secreted proteins (Figure 3E). In addition to chemokines and cytokines which signal and coordinate immune cell activities and inflammatory response (eg *Cxcl2*, *Ccl2*, *Il1b*, and *Il6*), several proteinases (eg *Mmp3* and *Mmp12*, as mentioned) and their inhibitors (*Timp1*, *Serpine1*, and *Serpinb2*) were highly expressed to orchestrate the tissue repair process. We also found two collagen encoding genes, *Col1a1* and *Col3a1*, which are known as fibrillar forming collagens that form connective tissues in skin (Figure 3E). Their high expression, approximately 10 000 sFPKM for both, at 6 days after incising is consistent with the histological finding of newly synthesized collagen tissue in the dermal layer at 6 and 12 days after incising as seen in the Masson's trichrome stained tissue (Figure 3A). At 1 day after incising, *S100a8* and *S100a9*,

TABLE 2 Top 50 differentially induced genes through the observed timepoints

Gene symbol	Gene name	sFPKM							Expression ratio compared to Unt
		Unt	1 hr	6 hr	1 d	3 d	6 d	12 d	
Nppb	Natriuretic peptide B	0.2	0.1	44.4	152.6	15.0	0.8	7.6	1017.1
Tnn	Tenascin N	0.3	0.4	1.1	7.9	238.1	114.9	98.6	882.0
Krt17	Keratin 17	10.1	10.1	1577.4	8747.5	2017.5	116.8	856.4	868.7
Il6	Interleukin 6	0.1	55.0	93.8	13.3	7.4	3.0	1.7	781.8
Cxcl2	C-X-C motif chemokine ligand 2	0.2	105.3	63.9	60.4	11.6	2.9	9.7	657.9
Cxcl1	C-X-C motif chemokine ligand 1	0.9	468.4	80.0	33.7	7.0	2.6	5.0	514.8
Stfa2l1	Stefin A2-like 1	0.2	0.6	73.5	61.2	14.8	0.7	3.3	408.3
Cxcl3	C-X-C motif chemokine ligand 3	0.1	1.1	41.5	28.7	7.3	1.6	5.8	345.8
S100a9	S100 calcium-binding protein A9	20.9	470.6	2417.2	5075.9	1354.9	133.6	591.2	242.4
Slpi	Secretory leukocyte peptidase inhibitor	4.0	20.8	742.6	817.6	574.7	181.0	348.3	202.4
Klk6	Kallikrein related-peptidase 6	0.3	0.1	2.9	34.2	47.2	2.7	23.4	188.8
Sh2d5	SH2 domain containing 5	0.1	0.1	10.8	19.3	2.3	0.3	0.9	175.5
Ptx3	Pentraxin 3	1.1	12.2	184.4	83.3	25.6	7.7	7.9	170.7
Reg3g	Regenerating family member 3 gamma	0.1	0.1	22.8	3.5	0.9	0.2	0.2	163.0
S100a8	S100 calcium-binding protein A8	23.9	129.9	1126.9	3585.5	996.8	117.8	576.5	150.2
Stfa2l2	Stefin A2-like 2	10.7	18.5	363.3	1568.6	319.1	37.5	61.0	146.3
Gip	Gastric inhibitory polypeptide	0.1	0.1	0.9	17.5	9.0	0.8	1.2	145.4
Stfa2	Stefin A2	42.2	57.7	1177.8	5359.0	1416.7	193.1	293.8	127.1
Stfa3	Stefin A3	36.3	24.4	340.5	4522.3	3008.5	1512.6	738.5	124.5
Ifnk	Interferon kappa	0.1	0.1	7.3	15.7	3.0	2.1	0.8	121.0
Defb4	Defensin beta 4	1.3	2.4	101.5	138.2	77.5	25.0	52.0	110.5
Nat8l	N-acetyltransferase 8-like	0.4	0.3	14.6	40.3	6.7	1.3	2.1	108.8
Il24	Interleukin 24	1.8	3.0	55.7	167.8	10.2	2.6	7.7	91.7
Ear1	Eosinophil-associated, ribonuclease A family, member 1	0.1	0.1	0.2	12.2	5.1	0.5	1.5	87.1
Areg	Amphiregulin	1.1	1.7	32.2	94.5	8.1	1.4	8.9	85.9
Mmp12	Matrix metallopeptidase 12	0.3	0.2	7.8	24.2	22.7	16.4	23.4	75.5
Slc6a14	Solute carrier family 6 member 14	0.1	0.2	10.5	9.5	1.9	0.4	3.1	75.1
Il1b	Interleukin 1 beta	2.0	68.1	141.7	62.3	25.5	10.6	24.3	69.8
Tarm1	T cell-interacting, activating receptor on myeloid cells 1	0.1	0.8	7.7	1.2	0.4	0.2	0.2	64.4

(Continues)

TABLE 2 (Continued)

Gene symbol	Gene name	sFPKM							Expression ratio compared to Unt
		Unt	1 hr	6 hr	1 d	3 d	6 d	12 d	
Fcar	Fc fragment of iga receptor	0.1	2.1	8.2	1.8	0.4	0.1	0.3	62.8
Hmox1	Heme oxygenase 1	17.9	20.1	1125.7	346.3	354.4	93.4	110.5	62.7
Mcemp1	Mast cell-expressed membrane protein 1	0.8	9.7	45.0	10.9	4.0	1.2	2.4	60.0
Ccl12	C-C motif chemokine ligand 12	0.2	0.2	11.7	5.7	9.0	4.9	3.0	58.7
Fcrl2	Fc receptor-like 2	1.3	1.3	0.6	11.4	73.5	31.2	26.9	57.4
Fosb	Fosb proto-oncogene, AP-1 transcription factor subunit	4.3	245.8	2.6	1.5	3.0	5.5	4.3	56.8
Osm	Oncostatin M	0.4	9.4	23.4	4.4	3.2	1.1	2.0	54.4
Sirpb2l1	Signal-regulatory protein beta 2-like 1	0.4	1.8	19.8	6.6	1.9	0.4	1.1	53.5
Cxcl6	C-X-C motif chemokine ligand 6	0.1	0.1	5.8	3.1	1.3	0.4	0.7	53.0
Fcnb	Ficolin B	4.6	8.8	231.0	29.7	21.2	5.2	4.8	50.0
Oscar	Osteoclast associated, immunoglobulin-like receptor	0.3	1.8	16.4	5.0	3.3	0.6	0.9	49.7
Krt71	Keratin 71, type II	0.2	0.1	0.9	10.4	4.2	0.7	1.5	49.5
Tmprss4	Transmembrane protease, serine 4	0.3	0.2	0.6	13.6	7.2	2.2	2.5	48.6
Angptl4	Angiopoietin-like 4	0.6	1.1	14.6	27.2	21.8	3.1	6.5	47.7
Ccl3	C-C motif chemokine ligand 3	2.1	41.0	99.8	56.1	30.4	8.0	11.8	46.6
Serpinb3	Serpin family B member 3	0.9	0.9	14.3	35.8	39.3	28.8	42.2	44.9
Rbp1	Retinol-binding protein 1	2.5	2.5	7.8	108.0	74.6	18.5	33.8	43.7
Mt2A	Metallothionein 2A	49.5	324.9	2068.9	652.2	312.8	106.5	117.4	41.8
Uox	Urate oxidase	2.1	0.8	58.2	84.5	56.0	10.9	21.8	41.0
Ccl7	C-C motif chemokine ligand 7	10.0	99.1	402.9	213.6	97.1	52.7	49.1	40.2
Hist1h2bk	Histone cluster 1, h2bk	0.3	0.3	0.6	10.2	10.4	1.7	1.8	40.0

Note: Although the actual sFPKM values of measurement had two decimal places, the values were rounded off and expressed using one decimal place in this table. The expression ratio was calculated using the actual values. The actual values are found in Table S1.

Abbreviations: d, day(s); hr, hours; Unt, untreated control.

FASEB JOURNAL

(A) Transcriptome elevation in subcellular components

(B) Secretome transcripts

(C) Time course of incisional secretome

(D) Top 30 expression ratio in secretome

FIGURE 2 Subcellular location of the differentially expressed genes (DEGs) and genes in the incisional secretome. A, The number (left) and proportion (right) of genes in six categories: secreted, extracellular, plasma membrane, cytoplasm, nucleus, and uncharacterized/other. B, Heatmap of the incisional secretome. C, The DEGs in the secretome at each timepoint with several representative genes labeled. For the scatter plot, the expression ratio between each timepoint and untreated control is plotted versus average sFPKM using logarithmic scales. D, The top 50 DEGs in the incisional secretome. Genes are arranged according to time after incision. Note the stepwise temporal patterns of transcript increases in B and D. d, day(s); hr or h, hour(s); Unt, untreated control

TABLE 3 Subcellular location

	Unt	1 hr	6 hr	1 d	3 d	6 d	12 d	Total
Number								
Secreted	22	45	65	52	69	131	58	442
Extracellular	46	60	55	92	70	144	65	532
Plasma membrane	92	132	191	215	262	294	140	1326
Cytoplasm	297	406	579	1121	980	1046	426	4855
Nucleus	189	210	395	947	514	516	200	2971
Uncategorized/ other	12	15	30	37	46	30	18	188
Proportion								
Secreted	3.3	5.2	4.9	2.1	3.6	6.1	6.4	4.3
Extracellular	7.0	6.9	4.2	3.7	3.6	6.7	7.2	5.2
Plasma membrane	14.0	15.2	14.5	8.7	13.5	13.6	15.4	12.9
Cytoplasm	45.1	46.8	44.0	45.5	50.5	48.4	47.0	47.1
Nucleus	28.7	24.2	30.0	38.4	26.5	23.9	22.1	28.8
Uncategorized/ other	1.8	1.7	2.3	1.5	2.4	1.4	2.0	1.8

Note: Although the actual sFPKM values of measurement had two decimal places, the values were rounded off and expressed using one decimal place in this table. The expression ratio was calculated using the actual values. The actual values are found in Table S1.

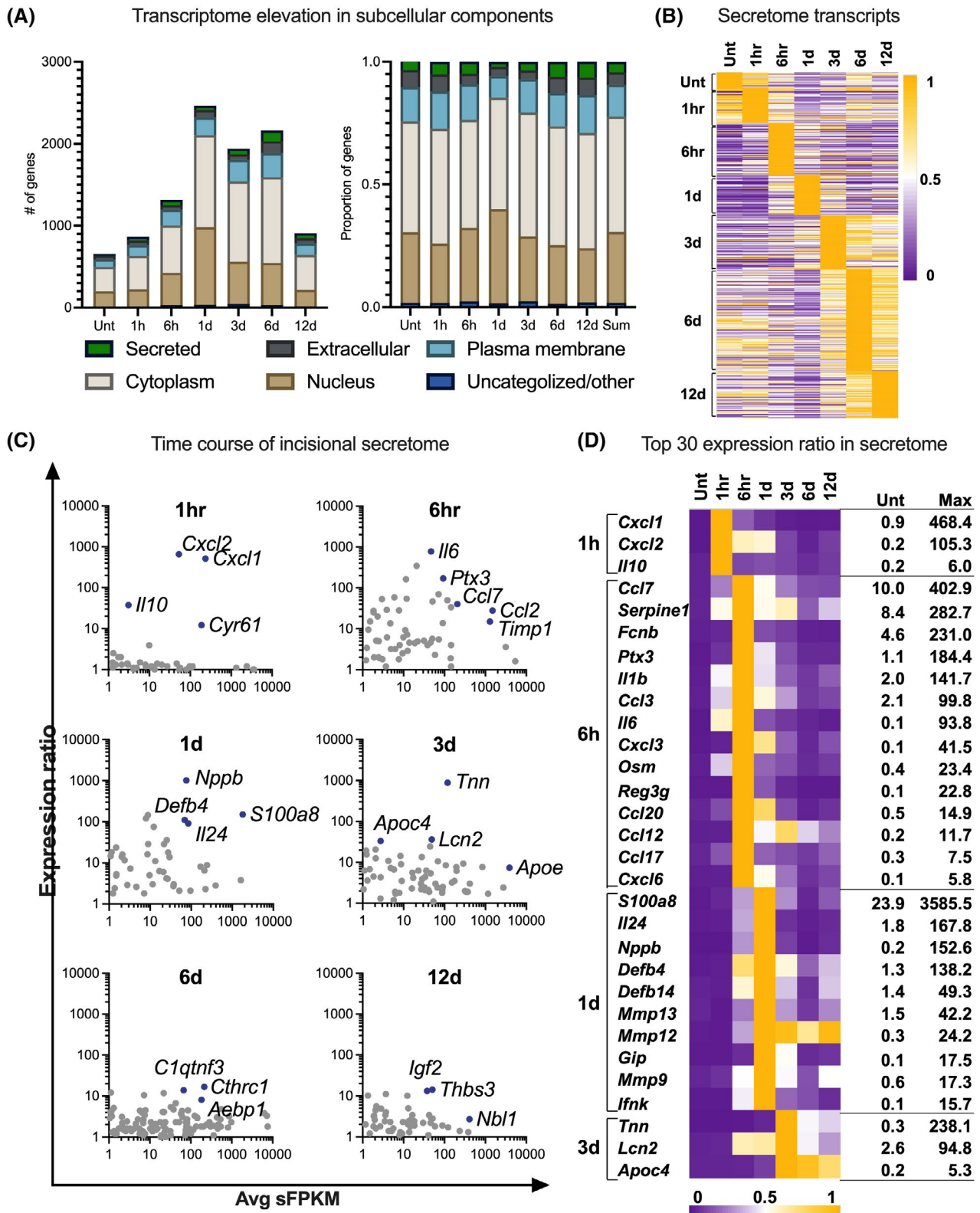Abbreviations: d, day(s); hr, hours; Unt, untreated control.

which are expressed in neutrophils[27] displayed a sharply elevated peak (Figure 3D). The in situ hybridization also showed the expression of *S100a9* in epidermal cells. Figure 3F shows localization of *S100a9* in the incised tissues at 6 hours and 1 day after incising. The signals were found in cells in both epidermal and dermal layers at both timepoints, but the signal in the epidermal layer increased to a peak between 6 hours and 1 day after incising. The signals in the epidermal layer were not found in the basal layer (Figure 3F right panel) but were specifically observed in the middle and upper layers.

3.4 | Transcripts related to sensory perception of pain

Among all the DEGs detected in this study, we identified 95 transcripts related to sensory processing or transduction of pain. Their temporal changes are indicated in Figure 4A,B. The most highly and DEGs were observed between 6 hours to 1 day after incising, and the largest number of genes occurred 6 hours after incising. To examine the altered expression in more detail, we extracted the 30 genes with the highest expression ratios (Figure 4C and Table 6) and those that encode secreted proteins (Figure 4D). Some examples of genes at each timepoint are shown in Figure 4E. The most rapidly induced

gene was *Il10* which was expressed maximally at 1 hour after incising, although the quantitative sFPKM values for *Il10* (6.0) was not the highest in the group of 30 genes. The expression of *Il10* was followed by *Ccl2* and *Ccl3* at 6 hours. At this time point, we also detected *Il1rn* and *Ngf* as high-differentially expressed as well as several receptors such as *Cxcr4*, *Cnr2* (cannabinoid receptor 2), *Ednrb* (endothelin receptor type B), and *Ptafr* (platelet activating factor receptor). At 1 day after incising, we detected *Gip* (gastric inhibitory polypeptide) as the most DEG in this category whose expression ratio was 145.4. The expression of *Ptgs2* (cyclooxygenase 2) was rapidly elevated from 1 hour to 1 day after incising as shown in Figure 4E.

3.5 | Transcripts related to synthesis and signaling of prosatnoids, eicosanoids, and other specialized pro-resolving lipid mediators (SPMs)

Oxidized lipids (oxylipins) have been shown to play a critical role in the formation of the water barrier in skin,[28-30] as well as in inflammation and the resolution of inflammation.[31-34] We hypothesized that transcripts might be induced to facilitate restoration. We examined the expression of 28 DEGs encoding enzymes that synthesize oxylipins involved in water barrier

TABLE 4 Top 30 differentially induced genes in the incision secretome

Gene symbol	Gene name	sFPKM Unt	1 hr	6 hr	1 d	3 d	6 d	12 d	Expression ratio compared to Unt
Nppb	Natriuretic peptide B	0.2	0.1	44.4	152.6	15.0	0.8	7.6	1017.1
Tnn	Tenascin N	0.3	0.4	1.1	7.9	238.1	114.9	98.6	882.0
Il6	Interleukin 6	0.1	55.0	93.8	13.3	7.4	3.0	1.7	781.8
Cxcl2	C-X-C motif chemokine ligand 2	0.2	105.3	63.9	60.4	11.6	2.9	9.7	657.9
Cxcl1	C-X-C motif chemokine ligand 1	0.9	468.4	80.0	33.7	7.0	2.6	5.0	514.8
Cxcl3	C-X-C motif chemokine ligand 3	0.1	1.1	41.5	28.7	7.3	1.6	5.8	345.8
Ptx3	Pentraxin 3	1.1	12.2	184.4	83.3	25.6	7.7	7.9	170.7
Reg3g	Regenerating family member 3 gamma	0.1	0.1	22.8	3.5	0.9	0.2	0.2	163.0
S100a8	S100 calcium-binding protein A8	23.9	129.9	1126.9	3585.5	996.8	117.8	576.5	150.2
Gip	Gastric inhibitory polypeptide	0.1	0.1	0.9	17.5	9.0	0.8	1.2	145.4
Ifnk	Interferon kappa	0.1	0.1	7.3	15.7	3.0	2.1	0.8	121.0
Defb4	Defensin beta 4	1.3	2.4	101.5	138.2	77.5	25.0	52.0	110.5
Il24	Interleukin 24	1.8	3.0	55.7	167.8	10.2	2.6	7.7	91.7
Mmp12	Matrix metallopeptidase 12	0.3	0.2	7.8	24.2	22.7	16.4	23.4	75.5
Il1b	Interleukin 1 beta	2.0	68.1	141.7	62.3	25.5	10.6	24.3	69.8
Ccl12	C-C motif chemokine ligand 12	0.2	0.2	11.7	5.7	9.0	4.9	3.0	58.7
Osm	Oncostatin M	0.4	9.4	23.4	4.4	3.2	1.1	2.0	54.4
Cxcl6	C-X-C motif chemokine ligand 6	0.1	0.1	5.8	3.1	1.3	0.4	0.7	53.0
Fcnb	Ficolin B	4.6	8.8	231.0	29.7	21.2	5.2	4.8	50.0
Ccl3	C-C motif chemokine ligand 3	2.1	41.0	99.8	56.1	30.4	8.0	11.8	46.6
Ccl7	C-C motif chemokine ligand 7	10.0	99.1	402.9	213.6	97.1	52.7	49.1	40.2
Il10	Interleukin 10	0.2	6.0	0.7	0.8	0.6	0.3	0.5	37.6
Lcn2	Lipocalin 2	2.6	3.4	58.9	61.3	94.8	45.3	28.7	36.3
Defb14	Defensin beta 14	1.4	0.8	28.3	49.3	19.0	3.1	19.3	36.0
Serpine1	Serpin family E member 1	8.4	151.2	282.7	151.0	172.7	47.4	110.4	33.7
Apoc4	Apolipoprotein C4	0.2	0.2	0.2	0.5	5.3	4.9	4.0	33.3
Ccl17	C-C motif chemokine ligand 17	0.3	1.1	7.5	1.3	1.0	0.6	1.3	28.9
Mmp9	Matrix metallopeptidase 9	0.6	1.1	8.6	17.3	8.5	2.4	8.7	28.8
Mmp13	Matrix metallopeptidase 13	1.5	0.2	10.1	42.2	12.6	3.4	11.1	28.5
Ccl20	C-C motif chemokine ligand 20	0.5	1.9	14.9	11.4	1.9	0.3	1.0	28.1

Note: Although the actual sFPKM values of measurement had two decimal places, the values were rounded off and expressed using one decimal place in this table. The expression ratio was calculated using the actual values. The actual values are found in Table S1.

Abbreviations: d, days; hr, hours; Max, maximum expression level; Unt, untreated control.
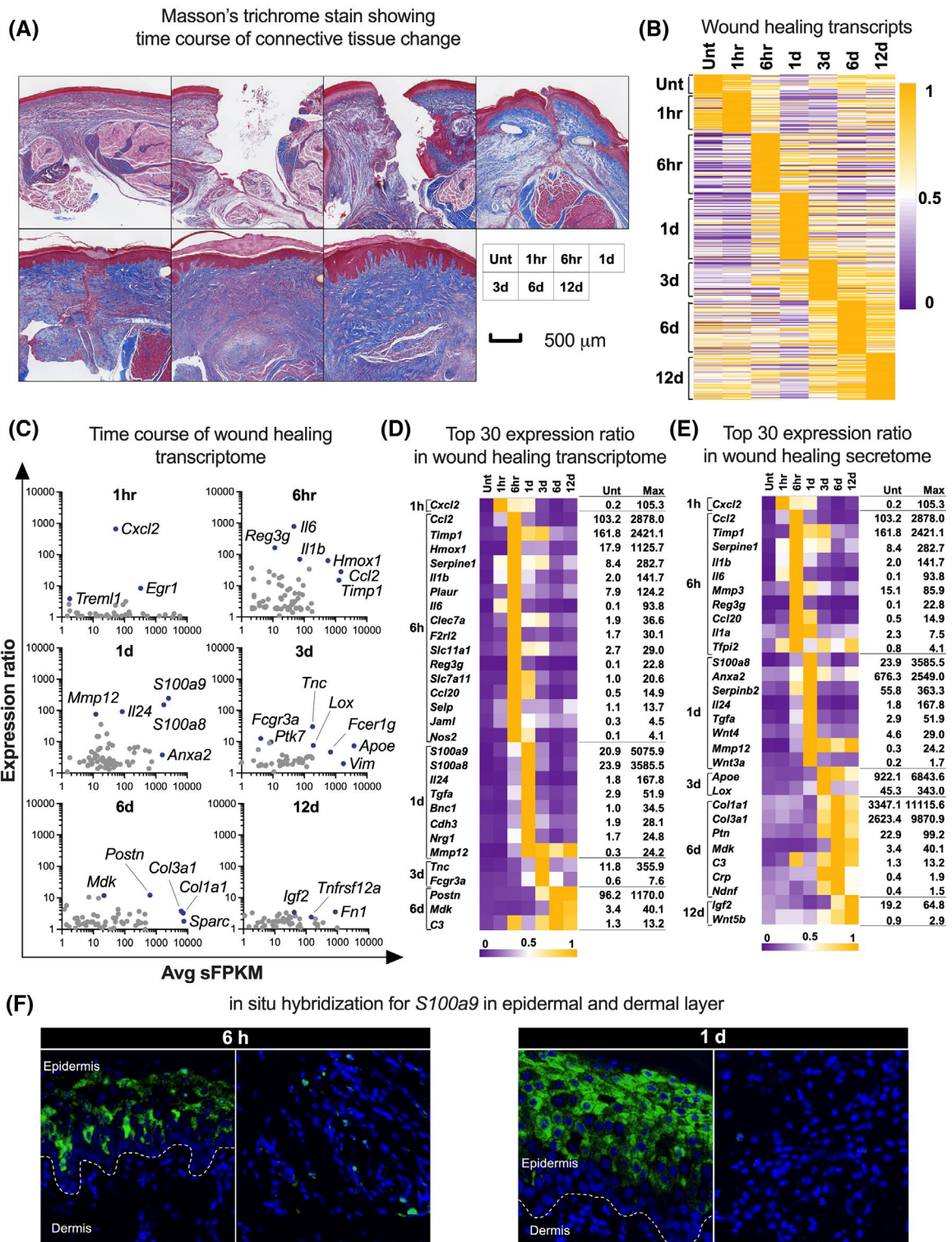
FIGURE 3 Extraction of transcripts related to wound healing using a gene ontology term. A, Photomicrographs of Masson's trichrome staining of incised hind paw tissues. B, Heatmap of the transcripts related to wound healing. C, The differentially expressed genes in the transcripts related to wound healing at each timepoint with several representative genes labeled. For the scatter plot, the expression ratio between each timepoint and untreated control is plotted versus average sFPKM using logarithmic scales. D, The top 30 differentially expressed transcripts related to wound healing. E, The top 30 differentially expressed transcripts of the wound-healing secretome. Note the stepwise temporal patterns of transcript increases in B, D and E. F, Photomicrographs of in situ hybridization for *S100a9* (green) and DAPI (blue) in the incised hind paw at 6 hours and 1 day after incising. Left panels in each timepoint shows the epidermis and the upper layer of dermis and right panels in each timepoint shows the middle layer of dermis. The vast majority of *S100a9* in situ signal is located in the epidermal layers. d, day(s); hr or h, hour(s); Unt, untreated control

THE FASEB JOURNAL

TABLE 5 Top 30 differentially induced transcripts related to wound healing

Gene symbol	Gene name	sFPKM							Expression ratio compared to Unt
		Unt	1 hr	6 hr	1d	3 d	6 d	12 d	
Il6	Interleukin 6	0.1	55.0	93.8	13.3	7.4	3.0	1.7	781.8
Cxcl2	C-X-C motif chemokine ligand 2	0.2	105.3	63.9	60.4	11.6	2.9	9.7	657.9
S100a9	S100 calcium-binding protein A9	20.9	470.6	2417.2	5075.9	1354.9	133.6	591.2	242.4
Reg3g	Regenerating family member 3 gamma	0.1	0.1	22.8	3.5	0.9	0.2	0.2	163.0
S100a8	S100 calcium-binding protein A8	23.9	129.9	1126.9	3585.5	996.8	117.8	576.5	150.2
Il24	Interleukin 24	1.8	3.0	55.7	167.8	10.2	2.6	7.7	91.7
Mmp12	Matrix metallopeptidase 12	0.3	0.2	7.8	24.2	22.7	16.4	23.4	75.5
Il1b	Interleukin 1 beta	2.0	68.1	141.7	62.3	25.5	10.6	24.3	69.8
Hmox1	Heme oxygenase 1	17.9	20.1	1125.7	346.3	354.4	93.4	110.5	62.7
Nos2	Nitric oxide synthase 2	0.1	0.1	4.1	2.6	0.3	0.2	0.3	37.0
Bnc1	Basonuclin 1	1.0	0.6	9.9	34.5	8.5	2.4	4.6	35.9
Serpine1	Serpin family E member 1	8.4	151.2	282.7	151.0	172.7	47.4	110.4	33.7
Tnc	Tenascin C	11.8	14.7	48.3	121.8	355.9	95.3	122.6	30.3
Ccl20	C-C motif chemokine ligand 20	0.5	1.9	14.9	11.4	1.9	0.3	1.0	28.1
Ccl2	C-C motif chemokine ligand 2	103.2	1083.2	2878.0	724.1	287.0	105.7	164.6	27.9
Slc7a11	Solute carrier family 7 member 11	1.0	1.0	20.6	16.5	4.9	1.4	2.4	21.6
Clec7a	C-type lectin domain family 7, member A	1.9	7.8	36.6	19.4	21.9	6.0	8.2	19.3
Tgfa	Transforming growth factor alpha	2.9	1.6	23.3	51.9	8.2	4.8	7.2	17.8
F2rl2	Coagulation factor II (thrombin) receptor-like 2	1.7	3.0	30.1	4.2	5.4	1.6	3.3	17.7
Jaml	Junction adhesion molecule like	0.3	1.4	4.5	2.3	1.9	1.3	1.5	16.2
Plaur	Plasminogen activator, urokinase receptor	7.9	22.5	124.2	43.6	30.3	18.4	40.9	15.7
Timp1	TIMP metallopeptidase inhibitor 1	161.8	227.3	2421.1	1805.8	2035.9	725.2	560.2	15.0
Nrg1	Neuregulin 1	1.7	1.2	12.2	24.8	5.1	1.7	4.2	14.7
Cdh3	Cadherin 3	1.9	1.5	9.6	28.1	10.6	5.1	5.5	14.7
Selp	Selectin P	1.1	4.2	13.7	4.4	4.5	2.6	6.1	12.8
Fcgr3a	Fc fragment of igg, low affinity iiia, receptor	0.6	0.7	0.9	3.7	7.6	3.8	1.7	12.7
Postn	Periostin	96.2	116.5	118.9	140.9	740.0	1170.0	1164.2	12.2
Mdk	Midkine	3.4	2.9	2.6	3.6	10.1	40.1	35.8	11.8
Slc11a1	Solute carrier family 11 member 1	2.7	4.3	29.0	17.6	16.3	5.6	5.4	10.9
C3	Complement component 3	1.3	2.1	11.7	4.4	9.9	13.2	11.2	10.5

Note: Although the actual sFPKM values of measurement had two decimal places, the values were rounded off and expressed using one decimal place in this table. The expression ratio was calculated using the actual values. The actual values are found in Table S1.

Abbreviations: d, days; hr, hours; Max, maximum expression level; Unt, untreated control.
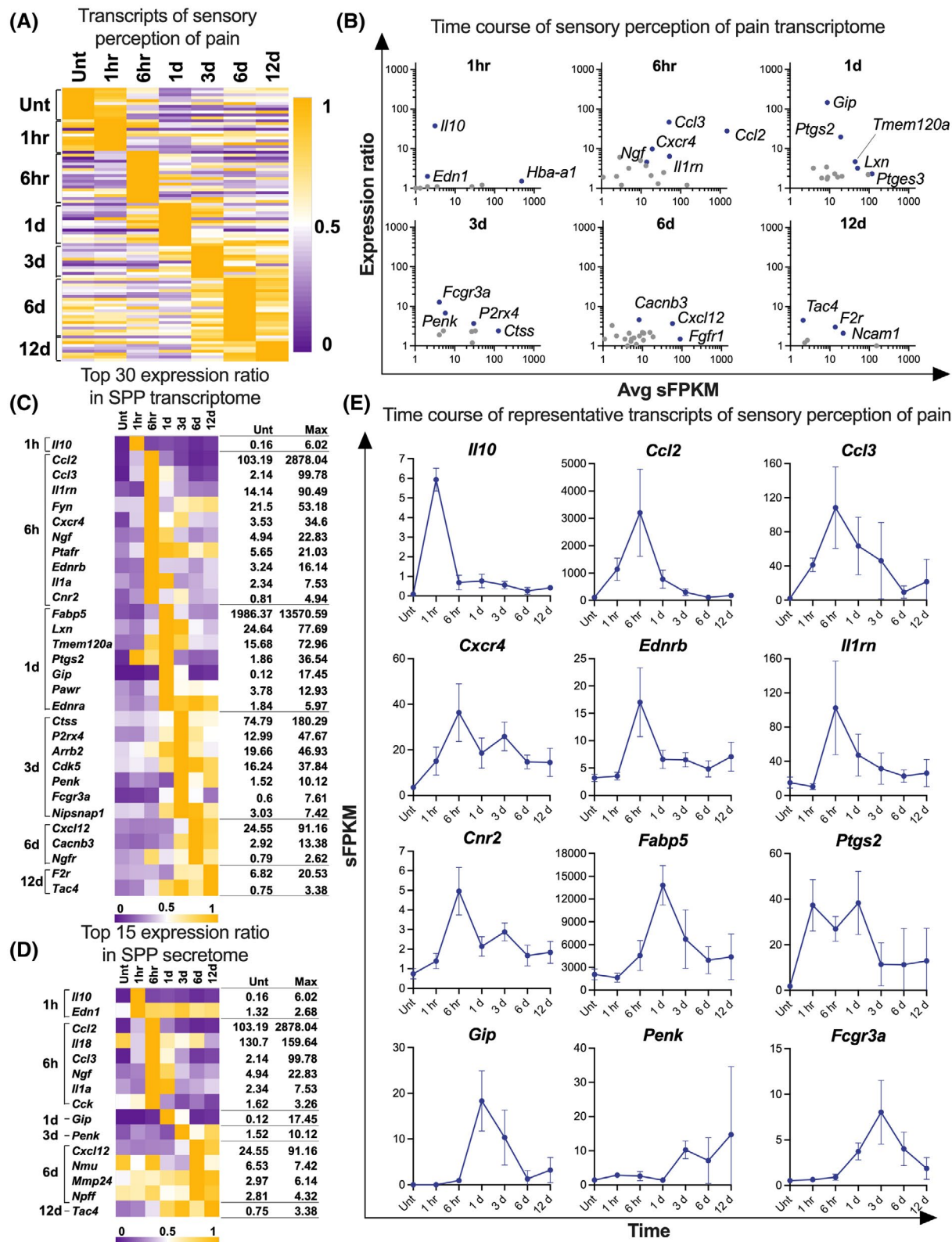
FIGURE 4 Extraction of transcripts related to sensory perception of pain using a GO term. A, Heatmap of the transcripts related to sensory perception of pain. B, The differentially expressed genes (DEGs) in the transcripts related to sensory perception of pain at each timepoint with several representative genes labeled. For the scatter plot, the expression ratio between each timepoint and untreated control is plotted versus average sFPKM using logarithmic scales. C, The top 30 DEGs in the transcripts related to sensory perception of pain. D, The DEGs in the sensory-perception-of-pain secretome. Note the temporal patterns of transcript increases in A, C, and D. E, Examples of high- DEGs at each timepoint. d, day(s); hr or h, hour(s); Unt, untreated control

TABLE 6 Top 30 differentially induced transcripts related to sensory perception of pain

Gene symbol	Gene name	sFPKM							Expression ratio compared to Unt
		Unt	1 hr	6 hr	1 d	3 d	6 d	12 d	
Gip	Gastric inhibitory polypeptide	0.1	0.1	0.9	17.5	9.0	0.8	1.2	145.4
Ccl3	C-C motif chemokine ligand 3	2.1	41.0	99.8	56.1	30.4	8.0	11.8	46.6
Il10	Interleukin 10	0.2	6.0	0.7	0.8	0.6	0.3	0.5	37.6
Ccl2	C-C motif chemokine ligand 2	103.2	1083.2	2878.0	724.1	287.0	105.7	164.6	27.9
Ptgs2	Prostaglandin-endoperoxide synthase 2	1.9	36.1	26.6	36.5	8.8	6.4	7.0	19.6
Fcgr3a	Fc fragment of igg, low affinity iiia, receptor	0.6	0.7	0.9	3.7	7.6	3.8	1.7	12.7
Cxcr4	C-X-C motif chemokine receptor 4	3.5	14.0	34.6	17.5	25.4	14.6	13.5	9.8
Fabp5	Fatty acid-binding protein 5, epidermal	1986.4	1564.8	4252.1	13 570.6	6060.4	3686.4	3512.8	6.8
Penk	Proenkephalin	1.5	2.9	2.4	1.5	10.1	5.4	8.0	6.7
Il1rn	Interleukin 1 receptor antagonist	14.1	10.0	90.5	42.5	28.1	21.8	20.9	6.4
Cnr2	Cannabinoid receptor 2	0.8	1.4	4.9	2.2	3.0	1.7	1.9	6.1
Ednrb	Endothelin receptor type B	3.2	3.6	16.1	6.5	6.5	4.8	6.8	5.0
Tmem120a	Transmembrane protein 120A	15.7	16.3	60.4	73.0	60.7	32.8	31.2	4.7
Ngf	Nerve growth factor	4.9	5.8	22.8	17.8	9.0	6.0	7.5	4.6
Cacnb3	Calcium voltage-gated channel auxiliary subunit beta 3	2.9	2.5	3.0	4.0	10.0	13.4	11.1	4.6
Tac4	Tachykinin 4 (hemokinin)	0.8	0.9	1.5	2.7	3.2	2.3	3.4	4.5
Ptafr	Platelet-activating factor receptor	5.7	9.2	21.0	19.7	18.7	12.2	15.6	3.7
Cxcl12	C-X-C motif chemokine ligand 12	24.6	22.0	23.0	23.9	42.3	91.2	76.7	3.7
P2rx4	Purinergic receptor P2X 4	13.0	12.8	20.3	28.7	47.7	32.1	24.1	3.7
Pawr	Pro-apoptotic WT1 regulator	3.8	2.9	5.6	12.9	6.8	7.1	6.5	3.4
Ngfr	Nerve growth factor receptor	0.8	0.9	2.0	1.2	1.5	2.6	1.7	3.3
Ednra	Endothelin receptor type A	1.8	1.5	2.1	6.0	5.3	5.8	5.0	3.2
Il1a	Interleukin 1 alpha	2.3	1.8	7.5	7.3	2.2	2.6	3.1	3.2
Lxn	Latexin	24.6	18.7	34.5	77.7	74.9	37.4	29.2	3.2
F2r	Coagulation factor II (thrombin) receptor	6.8	7.3	7.4	5.5	13.2	12.7	20.5	3.0
Fyn	FYN proto-oncogene, Src family tyrosine kinase	21.5	21.7	53.2	19.6	31.6	35.3	38.4	2.5
Nipsnap1	Nipsnap homolog 1 (C elegans)	3.0	3.2	2.3	5.4	7.4	7.2	4.9	2.4
Ctss	Cathepsin S	74.8	71.5	81.8	92.4	180.3	102.7	99.1	2.4
Arrb2	Arrestin, beta 2	19.7	22.6	27.4	41.4	46.9	28.8	22.2	2.4
Cdk5	Cyclin-dependent kinase 5	16.2	17.7	15.7	26.6	37.8	36.5	29.6	2.3

Note: Although the actual sFPKM values of measurement had two decimal places, the values were rounded off and expressed using one decimal place in this table. The expression ratio was calculated using the actual values. The actual values are found in Table S1.

Abbreviations: d, days; hr, hours; Max, maximum expression level; Unt, untreated control.
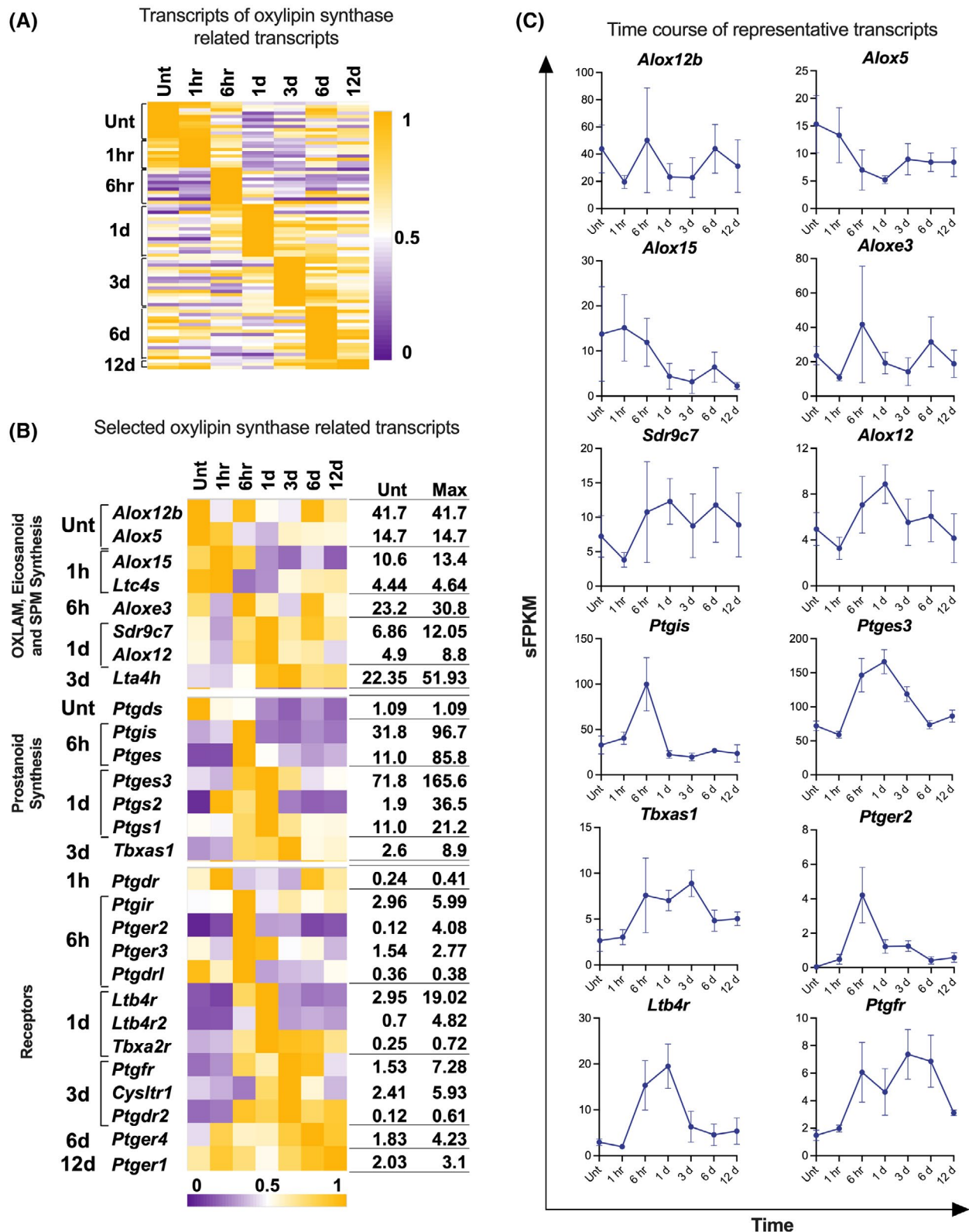
(A)

Transcripts of oxylipin synthase related transcripts

(B) Selected oxylipin synthase related transcripts

		Unt	1hr	6hr	1d	3d	6d	12d	Unt	Max
OXLAM, Eicosanoid and SPM Synthesis										
Unt	Alox12b								41.7	41.7
	Alox5								14.7	14.7
1h	Alox15								10.6	13.4
	Ltc4s								4.44	4.64
6h	Aloxe3								23.2	30.8
1d	Sdr9c7								6.86	12.05
	Alox12								4.9	8.8
3d	Lta4h								22.35	51.93
Prostanoid Synthesis										
Unt	Ptgds								1.09	1.09
6h	Ptgis								31.8	96.7
	Ptges								11.0	85.8
1d	Ptges3								71.8	165.6
	Ptgs2								1.9	36.5
	Ptgs1								11.0	21.2
3d	Tbxas1								2.6	8.9
Receptors										
1h	Ptgdr								0.24	0.41
6h	Ptgir								2.96	5.99
	Ptger2								0.12	4.08
	Ptger3								1.54	2.77
	Ptgdrl								0.36	0.38
1d	Ltb4r								2.95	19.02
	Ltb4r2								0.7	4.82
	Tbxa2r								0.25	0.72
3d	Ptgfr								1.53	7.28
	Cysltr1								2.41	5.93
	Ptgdr2								0.12	0.61
6d	Ptger4								1.83	4.23
12d	Ptger1								2.03	3.1

(C) Time course of representative transcripts

FIGURE 5 Extraction of transcripts related to synthesis and signaling of prosatnoids, eicosanoids and other specialized proresolving lipid mediators. A, Heatmap of the transcripts related to oxylipin synthesis. B, Heatmap of selected transcripts related to OXLAM, eicosanoid and SPM synthesis, prostanoid synthesis, and receptors. C, The time course of representative transcripts. d, day(s); hr or h, hour(s); SPM, specialized pro-resolving lipid mediator; Unt, untreated control
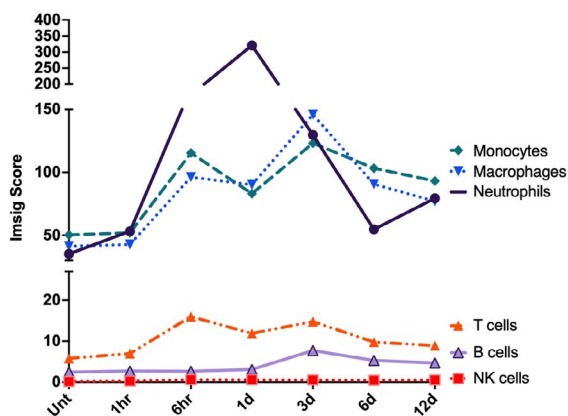
formation, pro-inflammatory lipid mediators (such as prostanoids) and SPMs. The temporal changes are indicated in Figure 5A. The most DEG was *Ptger2* (prostaglandin E receptor 2) (0.12 to 4.08 sFPKM). We further analyzed them based on the following three categories: (1) OXLAM, eicosanoid, and SPM synthesis, (2) prostanoid synthesis, and (3) receptors (Figure 5B). For the first category, half of the transcripts showed unchanged expression or downregulated patterns. *Alox12b* (arachidonate 12-lipoxygenase, 12R type) and *Aloxe3* (arachidonate lipoxygenase 3) showed unchanged but quite similar expression patterns (Figure 5C). *Alox5* (arachidonate lipoxygenase 5), *Alox15* (arachidonate lipoxygenase 15), and *Ltc4s* (leukotriene C4 synthase) were downregulated after incising (Figure 5B,C). For the second category, prostanoid synthesis, almost all of the transcripts were significantly upregulated after incising except for one gene, *Ptgds* (prostaglandin D2 synthase). Besides *Ptgs2* (discussed above) the most rapidly and highly upregulated prostanoid synthesis gene was *Ptges* (11.0 to 85.8 by

6 hours) (Prostaglandin E Synthase, Figure 5B). For the third category, receptors, almost all of the transcripts were upregulated within 1 day after incising. Several genes, particularly those encoding prostanoid receptors, had not recovered to their baseline levels by 12 days after incising (Figure 5B).
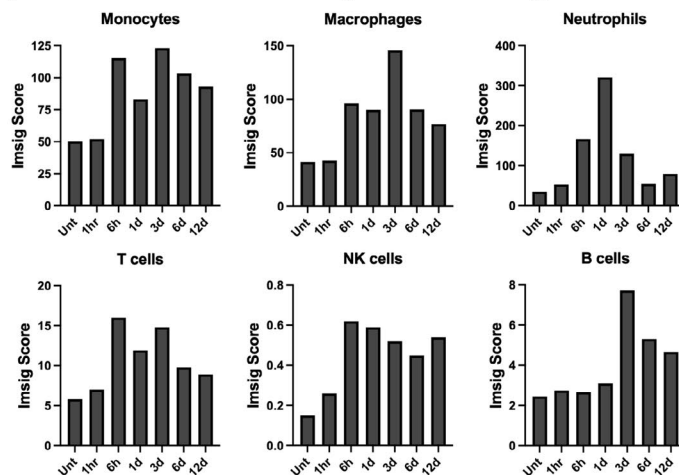
3.6 | Immune cell and pathway analysis

To examine immune cell activities and several pathways related to these cells, we utilized the Imsig R package. This analysis involves scoring for the presence of monocytes, macrophages, neutrophils, T-lymphocytes, NK cells, B-lymphocytes, as well as scoring for signaling or biosynthetic pathways including interferon, proliferation, and translation (Figure 6). Figure 6A shows temporal score changes in the immune cell types examined and the detailed score changes of each cell type are plotted in Figure 6B. The most infiltrated and/or activated immune cells were neutrophils

FIGURE 6 Immune cell and pathway analysis. A, Line graphs of the time course of relative levels of different immune cell types and pathways based on gene clusters for several populations in the incised hind paw. B, The detailed Imsig scores for all the categories are plotted as bar graphs. d, day(s); hr or h, hour(s); Unt, untreated control

which exhibited a sharp peak score at 1 day after incising. The scores and pattern for monocytes and macrophages were similar through the timepoints. They had a bimodal pattern with peaks at 6 hours and at day 3 after incising. T- and B-lymphocytes had a relatively low Imsig scores compared to monocytes, macrophages, and neutrophils. The peak representation for T-cells occurred at the 6-hour timepoint after incising and B-lymphocyte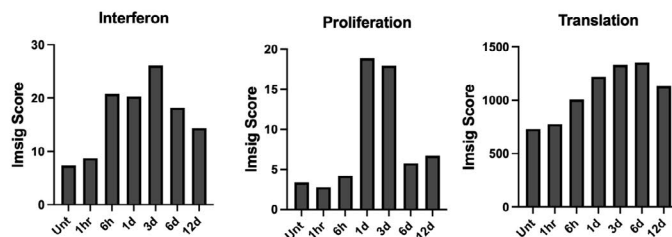s had their peak at 3 days. While NK cells also gradually increased over the times examined, their average score was also quite low. Figure 6C shows temporal score changes in the pathways examined and the detailed score changes of each pathway are plotted in Figure 6D. The score of the translational pathway gradually increased and its peak occurred at 6 days after incising. The average scores of the interferon and proliferation pathways were relatively low, and their peaks were at 3 days and 1 day after incising, respectively. The proliferation pathway was increased between 1 and 3 days after incising.

3.7 | Comparison of DEGs in the surgical incision model with the peripheral inflammation model

To explore gene profile characteristics specific to the incision transcriptome, we compared the dataset of the surgical incision model to a dataset of a peripheral inflammation model, which includes 3817 DEGs. We excluded a total of 897 uncharacterized genes from the latter dataset. The remaining 2920 genes were analyzed further. By comparing the two datasets, we detected 7647 incision-specific DEGs, 253 inflammation-specific DEGs, and 2667 common DEGs (Figure 7A). The temporal expression changes for the common genes are shown in Figure 7B, and the 50 common genes that had the highest expression ratio in the incision dataset are shown in Table 7. We defined "Induction Indexes" as averages of expression level in sFPKM (left graph in Figure 7C) and expression ratio (right graph in Figure 7C) in the two models. The average sFPKM was much higher in the incision model than the inflammation model while the expression ratios in the two models were highly correlated until 3 days after each intervention. At 3 days after incising, we observed decreased expression ratio in the incision model but slightly increased in the inflammation model. Figure 7D shows some selected genes that do (shared genes) or do not (incision distinct genes) have similar expression patterns between the two models. A scatter plot in Figure 7E shows the highest expression ratios in the two models plotted against each other that allows visualization of the shared genes and the genes distinct to the incision manipulation. Even within the shared genes, expression levels in the incision model were much higher

than those in the inflammation model (left column in Figure 7F). The incision-distinct genes had model specific expression patterns (right column in Figure 7F). Among the incision distinct genes, *Nppb* had the highest expression ratio not only in this group but in entire set of DEGs in the incision dataset (expression ratio = 1017.1 at 1 day after incising). We examined the location in control and incised hind paw tissue of *Nppb* and of its receptors, *Npr1* and *Npr3* using in situ hybridization (Figure 7G). In the incision model, *Nppb* was located in cells in the epidermal layer, specifically around the wound edges at 1 day after incision (the delocalized and non-dot, smear-like signals found mainly above the epidermal layer was determined as non-specific signals). *Npr1* was most highly expressed at 3 days after incising in the incision model. It was located broadly in both the basal epidermal layer and the dermal layer. Expression levels for *Npr3* gradually decreased after incising and this transcript was found mainly in the dermal and muscle layers (Figure S2) but also was found in the basal epidermal layer at 3 days after incising. These histological findings were consistent with the temporal changes in sFPKM values for each gene. Interestingly, there were nerve bundles that displayed *Npr3* signal in the tissue (Figure S2). While *Npr1* and *Npr3* were not differentially expressed in the inflammation model, in situ hybridization detected them located in similar regions as in the incision model. At 3 days after inducing inflammation, *Npr3* was also found at the epidermal layer.

Figure 8A shows temporal expression changes in the incision specific DEGs. Genes that had peak expression at 1 hour after incising or in the untreated control were dramatically downregulated between 1 and 3 days after incising. The largest population of incision-specific genes had their peak expression at 1 day after incising (Figure 8B). However, at this time, we observed a decrease in the transcription of genes encoding secreted proteins, whereas transcription of genes located in the cytoplasm and nucleus were dramatically increased at this time (Figure 2A and Table 3). These results may indicate that many important biological processes related to incising occur approximately one day after incising. Figure 8C and Table 8 show 50 genes that had the highest expression ratio, three of which had more than a 100-fold expression ratio. These were *Klk6* (kallikrein-related–peptidase 6), a serine protease, *Stfa3* (stefin A3, cystatin A), an intracellular thiol proteinase inhibitor, and *Gip* (gastric inhibitory polypeptide), having an important role for insulin secretion. Figure 8D and Table 9 show the 50 genes of the incision-specific secretome that had the highest expression ratios. In the tissue repair phase, of the 12 genes that had their peak expression at 6 days after incising, we found that the majority encoded secreted peptidases, examples being *Mmp2*, *Aebp1*, *Mmp23*, *Adamts7*, and *Adamtsl1*.

(A) Number of DEGs in two models **(D)** Shared and distinct transcripts **(F)** Representitive transcripts of hared and distinct transcripts

(B) Transcripts of common genes

(C) Induction Indexes

(E) Scatter plot of shared and distinct transcripts
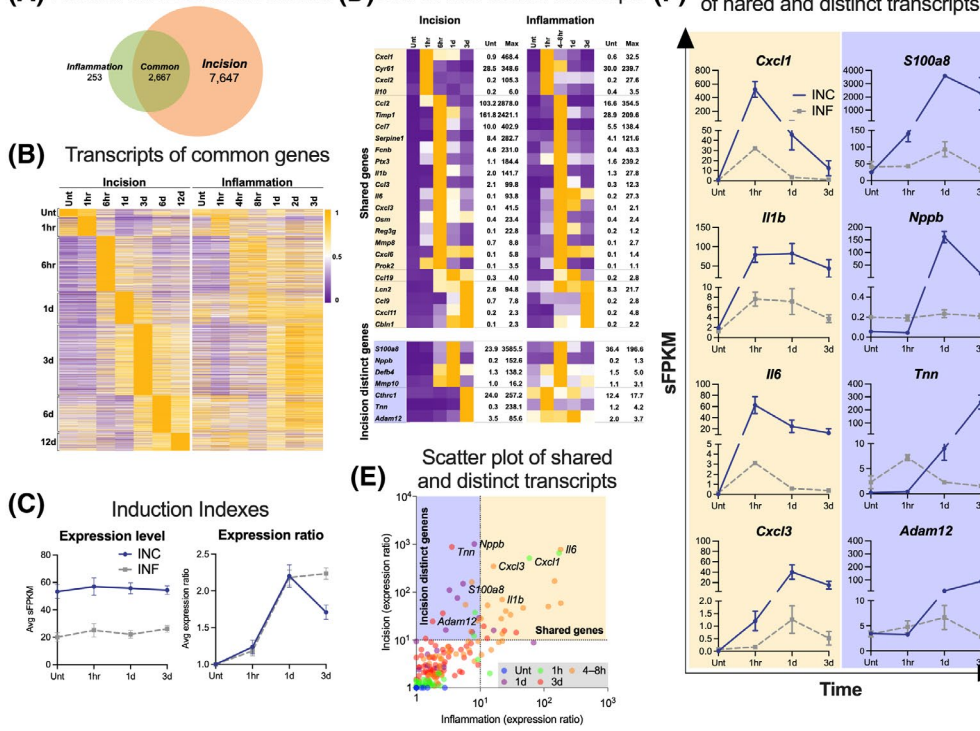
(G) in situ hybridization for *Npr1*, *Npr3*, and *Nppb*
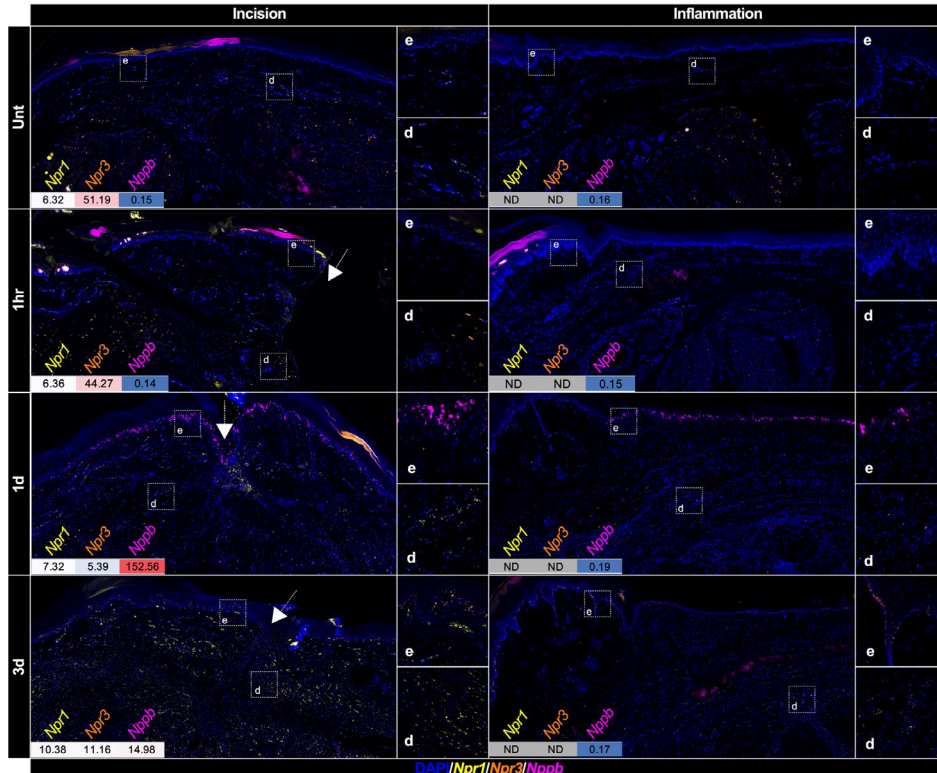
4 | DISCUSSION

The present study investigates the biological modifications regulating hyperalgesia, immune system reactivity and the healing process of incised tissue by delineating molecular dynamics and histological tissue changes occurring at the site of the surgical incision, and hyperalgesic behavioral responses that ensue. To identify molecular targets for new analgesics and for promoting healing process, locally induced transcriptomic profiles in the injured tissue were closely examined from the perspectives of temporal expression changes, subcellular locations, secreted gene products,

FIGURE 7 Comparison of differentially expressed gens between the surgical incision and the peripheral inflammation models. A, The number of common and model-specific differentially expressed genes. B, Temporally arranged heatmap of all genes in the common category in the two models. C, Induction Indexes were defined as averages of expression level in sFPKM (left) and expression ratio (right graph) in the two models. The expression level graph shows overall greater induction in the incision model. The expression ratio graph shows similar induction patterns the two manipulations, but they begin to diverge at day 3. The time course on the X-axis goes out to 3 days because the inflammation experiment was terminated at that time. D, Some examples of genes that have overlapping temporal expression patterns between the two models ("shared genes" in right yellow background) and that have distinct temporal patterns in the incision model ("incision distinct genes" in right purple background). E, Scatter plot showing the expression ratios in the incision model plotted against the expression ratio in the inflammation model at the different timepoints. The yellow background at the right indicates the shared genes, and the left purple background indicates the incision distinct genes. Note that *S100a8* is elevated in both conditions but the increase is substantially greater after incision and the specific increase in *Nppb* transcript in the incision model (see plots in panel F). F, Some examples of the shared genes (right yellow background) and the incision distinct genes (right purple background). G, Photomicrographs of in situ hybridization over time for *Nppb* (magenta), and the receptors for *Nppb*, *Npr1* (yellow), *Npr3* (orange), and DAPI (blue) in the incised hind paw (left column) compared to the inflammation (right column). The values with heatmap in the left bottom of each image show sFPKM of each target gene. Small insets at the right side of each column show high power images of epidermal layer (e) and dermal layer (d) of the boxed regions in each low power image. White arrows indicate incision sites. In four panels, the cornified epithelial layer contains some non-specific magenta or orange fluorescence and these sites do not represent the presence of transcript. d, day(s); hr or h, hour(s); Unt, untreated control

TABLE 7 Top 50 differentially expressed common genes between the incision and inflammation models

Gene symbol	Gene name	Incision			Inflammation		
		Unt	Max	Expression ratio compared to Unt	Unt	Max	Expression ratio compared to Unt
Nppb	Natriuretic peptide B	0.2	152.6	1017.1	0.2	2.4	15.1
Tnn	Tenascin N	0.3	238.1	882.0	1.2	4.2	3.6
Krt17	Keratin 17	10.1	8747.5	868.7	36.2	156.5	4.3
Il6	Interleukin 6	0.1	93.8	781.8	0.2	29.9	199.3
Cxcl2	C-X-C motif chemokine ligand 2	0.2	105.3	657.9	0.2	27.6	172.3
Cxcl1	C-X-C motif chemokine ligand 1	0.9	468.4	514.8	0.6	36.7	66.8
Stfa2l1	Stefin A2-like 1	0.2	73.5	408.3	0.2	3.6	15.5
Cxcl3	C-X-C motif chemokine ligand 3	0.1	41.5	345.8	0.1	2.5	19.2
S100a9	S100 calcium-binding protein A9	20.9	5075.9	242.4	1.5	249.0	169.4
Slpi	Secretory leukocyte peptidase inhibitor	4.0	817.6	202.4	4.9	44.6	9.1
Sh2d5	SH2 domain containing 5	0.1	19.3	175.5	0.1	2.4	22.0
Ptx3	Pentraxin 3	1.1	184.4	170.7	1.6	283.8	174.1
Reg3g	Regenerating family member 3 gamma	0.1	22.8	163.0	0.2	2.2	13.8
S100a8	S100 calcium-binding protein A8	23.9	3585.5	150.2	36.4	310.7	8.5
Stfa2l2	Stefin A2-like 2	10.7	1568.6	146.3	10.5	45.7	4.3
Stfa2	Stefin A2	42.2	5359.0	127.1	30.8	164.2	5.3
Ifnk	Interferon kappa	0.1	15.7	121.0	0.1	0.4	2.6
Defb4	Defensin beta 4	1.3	138.2	110.5	1.5	8.1	5.3
Nat8l	N-acetyltransferase 8-like	0.4	40.3	108.8	6.2	17.0	2.8
Ear1	Eosinophil-associated, ribonuclease A family, member 1	0.1	12.2	87.1	0.2	0.5	2.4
Areg	Amphiregulin	1.1	94.5	85.9	0.1	0.6	4.8
Mmp12	Matrix metallopeptidase 12	0.3	24.2	75.5	0.5	2.6	5.3
Slc6a14	Solute carrier family 6 member 14	0.1	10.5	75.1	0.7	2.4	3.7

(Continues)

TABLE 7 (Continued)

| Gene symbol | Gene name | Incision | | | Inflammation | | |
		Unt	Max	Expression ratio compared to Unt	Unt	Max	Expression ratio compared to Unt
Il1b	Interleukin 1 beta	2.0	141.7	69.8	1.3	36.5	28.9
Tarm1	T cell-interacting, activating receptor on myeloid cells 1	0.1	7.7	64.4	0.1	1.3	11.7
Fcar	Fc fragment of iga receptor	0.1	8.2	62.8	0.1	1.0	8.2
Hmox1	Heme oxygenase 1	17.9	1125.7	62.7	19.3	338.4	17.5
Mcemp1	Mast cell-expressed membrane protein 1	0.8	45.0	60.0	0.2	4.0	23.3
Ccl12	C-C motif chemokine ligand 12	0.2	11.7	58.7	0.2	33.0	183.1
Fosb	Fosb proto-oncogene, AP-1 transcription factor subunit	4.3	245.8	56.8	5.1	67.8	13.2
Sirpb2l1	Signal-regulatory protein beta 2-like 1	0.4	19.8	53.5	0.1	2.8	19.8
Cxcl6	C-X-C motif chemokine ligand 6	0.1	5.8	53.0	0.1	1.6	14.2
Fcnb	Ficolin B	4.6	231.0	50.0	0.4	51.9	140.4
Oscar	Osteoclast associated, immunoglobulin-like receptor	0.3	16.4	49.7	0.1	2.8	25.1
Ccl3	C-C motif chemokine ligand 3	2.1	99.8	46.6	0.3	15.9	61.2
Ccl7	C-C motif chemokine ligand 7	10.0	402.9	40.2	5.5	150.7	27.4
Csf3r	Colony stimulating factor 3 receptor	1.9	75.8	39.3	0.2	10.8	51.4
Irg1	Immunoresponsive gene 1	0.1	4.0	36.7	0.1	4.3	39.5
Serpine1	Serpin family E member 1	8.4	282.7	33.7	4.1	176.4	43.3
Clec4a2	C-type lectin domain family 4, member A2	0.6	14.3	24.6	0.2	18.4	79.9
Cd300ld	Cd300 molecule-like family member D	1.2	23.6	19.2	0.2	9.7	54.0
Lilrb3	Leukocyte immunoglobulin like receptor B3	0.3	5.6	17.6	0.8	71.3	85.9
Hk3	Hexokinase 3	0.3	5.6	17.6	0.2	19.1	82.8
Sell	Selectin L	2.5	39.3	15.8	0.2	18.5	84.3
Fcgr3a	Fc fragment of igg, low affinity iiia, receptor	0.6	7.6	12.7	0.2	14.0	63.6
Ebi3	Epstein-Barr virus induced 3	1.0	11.7	12.2	0.2	13.0	56.7
Spp1	Secreted phosphoprotein 1	49.4	434.8	8.8	5.2	956.4	182.5
Mx1	Myxovirus (influenza virus) resistance 1	1.3	10.0	8.0	1.5	121.0	79.1
Ankrd1	Ankyrin repeat domain 1	22.7	179.2	7.9	0.6	54.7	91.1
Ankrd2	Ankyrin repeat domain 2	21.2	81.4	3.9	0.2	21.3	118.1

Note: Although the actual sFPKM values of measurement had two decimal places, the values were rounded off and expressed using one decimal place in this table. The expression ratio was calculated using the actual values. The actual values are found in Table S1.

Abbreviations: Max, maximum expression level; Unt, untreated control.

wound healing, immune cell profiles, and comparison with peripheral inflammation. Superimposed on the genetic and cellular alterations were relevant modulations of behavioral nociceptive sensitivity leading to hyperalgesia and allodynia. We extended the time course to capture the complete process of wound inception and wound healing from both histological and molecular profile perspectives. All the DEGs detected in the present study are listed in the Table S1.

To validate our results externally, we referred to a previous study that performed microarray in the surgical incision model.[35] First, we confirmed that we had similar hyperalgesic behavioral patterns for both mechanical and thermal tests. Furthermore, in terms of major proinflammatory cytokine expressions, the microarray study showed that *Il6* had a peak at 1 hour after incising in the skin and at 4 hours in the muscle layer, and *Il1b* had a peak through 4 to 24 hours after incising in both skin and muscle. In our dataset, *Il6* was increased from 1 hour and had a peak at 6 hours after incising, and *Il1b* also increased from 1 hour, had a peak at 6 hours, and gradually decreased through
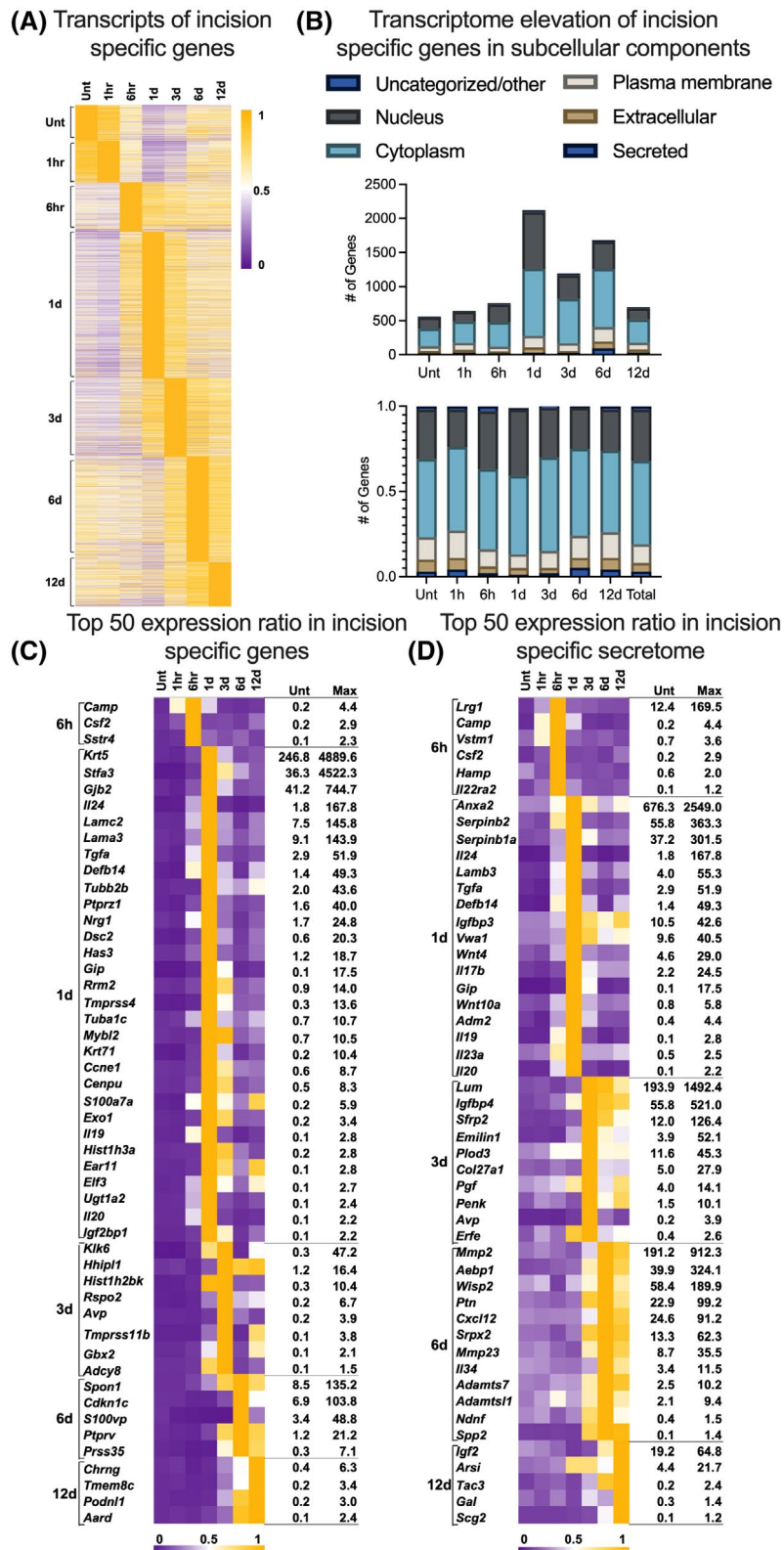
(A) Transcripts of incision specific genes

(B) Transcriptome elevation of incision specific genes in subcellular components

- Uncategorized/other
- Nucleus
- Cytoplasm
- Plasma membrane
- Extracellular
- Secreted

(C) Top 50 expression ratio in incision specific genes

	Gene	Unt	Max
6h	Camp	0.2	4.4
	Csf2	0.2	2.9
	Sstr4	0.1	2.3
	Krt5	246.8	4889.6
	Stfa3	36.3	4522.3
	Gjb2	41.2	744.7
	Il24	1.8	167.8
	Lamc2	7.5	145.8
	Lama3	9.1	143.9
	Tgfa	2.9	51.9
	Defb14	1.4	49.3
	Tubb2b	2.0	43.6
	Ptprz1	1.6	40.0
	Nrg1	1.7	24.8
	Dsc2	0.6	20.3
	Has3	1.2	18.7
	Gip	0.1	17.5
1d	Rrm2	0.9	14.0
	Tmprss4	0.3	13.6
	Tuba1c	0.7	10.7
	Mybl2	0.7	10.5
	Krt71	0.2	10.4
	Ccne1	0.6	8.7
	Cenpu	0.5	8.3
	S100a7a	0.2	5.9
	Exo1	0.2	3.4
	Il19	0.1	2.8
	Hist1h3a	0.2	2.8
	Ear11	0.1	2.8
	Elf3	0.1	2.7
	Ugt1a2	0.1	2.4
	Il20	0.1	2.2
	Igf2bp1	0.1	2.2
	Klk6	0.3	47.2
	Hhipl1	1.2	16.4
	Hist1h2bk	0.3	10.4
3d	Rspo2	0.2	6.7
	Avp	0.2	3.9
	Tmprss11b	0.1	3.8
	Gbx2	0.1	2.1
	Adcy8	0.1	1.5
	Spon1	8.5	135.2
	Cdkn1c	6.9	103.8
6d	S100vp	3.4	48.8
	Ptprv	1.2	21.2
	Prss35	0.3	7.1
	Chrng	0.4	6.3
12d	Tmem8c	0.2	3.4
	Podnl1	0.2	3.0
	Aard	0.1	2.4

(D) Top 50 expression ratio in incision specific secretome

	Gene	Unt	Max
6h	Lrg1	12.4	169.5
	Camp	0.2	4.4
	Vstm1	0.7	3.6
	Csf2	0.2	2.9
	Hamp	0.6	2.0
	Il22ra2	0.1	1.2
	Anxa2	676.3	2549.0
	Serpinb2	55.8	363.3
	Serpinb1a	37.2	301.5
	Il24	1.8	167.8
	Lamb3	4.0	55.3
	Tgfa	2.9	51.9
	Defb14	1.4	49.3
	Igfbp3	10.5	42.6
1d	Vwa1	9.6	40.5
	Wnt4	4.6	29.0
	Il17b	2.2	24.5
	Gip	0.1	17.5
	Wnt10a	0.8	5.8
	Adm2	0.4	4.4
	Il19	0.1	2.8
	Il23a	0.5	2.5
	Il20	0.1	2.2
	Lum	193.9	1492.4
	Igfbp4	55.8	521.0
	Sfrp2	12.0	126.4
	Emilin1	3.9	52.1
3d	Plod3	11.6	45.3
	Col27a1	5.0	27.9
	Pgf	4.0	14.1
	Penk	1.5	10.1
	Avp	0.2	3.9
	Erfe	0.4	2.6
	Mmp2	191.2	912.3
	Aebp1	39.9	324.1
	Wisp2	58.4	189.9
	Ptn	22.9	99.2
	Cxcl12	24.6	91.2
	Srpx2	13.3	62.3
6d	Mmp23	8.7	35.5
	Il34	3.4	11.5
	Adamts7	2.5	10.2
	Adamtsl1	2.1	9.4
	Ndnf	0.4	1.5
	Spp2	0.1	1.4
	Igf2	19.2	64.8
	Arsi	4.4	21.7
12d	Tac3	0.2	2.4
	Gal	0.3	1.4
	Scg2	0.1	1.2

FIGURE 8 Surgical incision-specific differentially expressed genes (DEGs). A, Heatmap of surgical incision-specific genes. B, The number (upper) and proportion (lower) of genes in six categories in each cluster: secreted, extracellular, plasma membrane, cytoplasm, nucleus, and uncharacterized/other. C, The top 50 incision-specific DEGs. Seven colored boxes on the heatmap indicate each timepoint as same as in (A). D, The top 50 incision-specific secretome. Note the temporal step wise progression of gene expression in A, C, and D. Also note that in panel C, 1 day contains the highest representation of incision specific gene regulation. Sixty percent of the genes in the figure are maximally differentially regulated at this time point. d, day(s); hr or h, hour(s); Unt, untreated control

24 hours after incising (Figure 1H). These results are regarded as being consistent with the combined results of the skin and muscle from the previous study because the total RNA for our dataset was extracted from whole skin tissues including the underlying muscle, while the previous study divided the tissues into the skin and muscle.

The remainder of the discussion is divided into three temporal stages: initial (one hour to 1 day), middle 1 day to 3 days, and late (3 days to 12 days). These three periods exemplified the (1) rapidly evolving edema and hyperalgesia early molecular orchestration of the tissue response, (2) infiltration and accumulation of leukocyte populations,

TABLE 8 Top 50 differentially induced genes in incision-specific genes

Gene symbol	Gene name	sFPKM							Expression ratio compared to Unt
		Unt	1 hr	6 hr	1d	3 d	6 d	12 d	
Klk6	Kallikrein-related peptidase 6	0.3	0.1	2.9	34.2	47.2	2.7	23.4	188.8
Gip	Gastric inhibitory polypeptide	0.1	0.1	0.9	17.5	9.0	0.8	1.2	145.4
Stfa3	Stefin A3	36.3	24.4	340.5	4522.3	3008.5	1512.6	738.5	124.5
Il24	Interleukin 24	1.8	3.0	55.7	167.8	10.2	2.6	7.7	91.7
Krt71	Keratin 71, type II	0.2	0.1	0.9	10.4	4.2	0.7	1.5	49.5
Tmprss4	Transmembrane protease, serine 4	0.3	0.2	0.6	13.6	7.2	2.2	2.5	48.6
Hist1h2bk	Histone cluster 1, h2bk	0.3	0.3	0.6	10.2	10.4	1.7	1.8	40.0
Dsc2	Desmocollin 2	0.6	0.4	2.6	20.3	6.6	1.7	4.4	36.9
Defb14	Defensin beta 14	1.4	0.8	28.3	49.3	19.0	3.1	19.3	36.0
Tmprss11b	Transmembrane protease, serine 11B	0.1	0.1	0.1	0.8	3.8	0.2	2.8	34.5
Rspo2	R-spondin 2	0.2	0.2	0.3	1.6	6.7	2.5	3.1	33.7
S100a7a	S100 calcium-binding protein A7A	0.2	0.1	3.1	5.9	3.3	1.5	4.9	31.3
Ptprz1	Protein tyrosine phosphatase, receptor type Z1	1.6	1.1	5.1	40.0	8.5	4.1	5.4	25.7
Elf3	E74-like factor 3	0.1	0.1	1.0	2.7	1.4	0.5	1.6	24.5
Il19	Interleukin 19	0.1	0.1	1.6	2.8	0.4	0.1	0.3	23.7
Prss35	Protease, serine, 35	0.3	0.3	0.1	0.2	4.0	7.1	5.5	22.9
Tubb2b	Tubulin, beta 2B class iib	2.0	2.7	2.5	43.6	17.8	13.5	23.6	22.1
Igf2bp1	Insulin-like growth factor 2 mrna-binding protein 1	0.1	0.1	0.2	2.2	1.3	0.2	0.5	21.8
Avp	Arginine vasopressin	0.2	0.2	0.2	0.3	3.9	0.9	0.4	20.7
Earl1	Eosinophil-associated, ribonuclease A family, member 11	0.1	0.1	0.2	2.8	2.2	0.8	2.4	20.2
Ugt1a2	UDP glucuronosyltransferase 1 family, polypeptide A2	0.1	0.1	0.9	2.4	0.3	0.2	0.3	20.2
Camp	Cathelicidin antimicrobial peptide	0.2	2.5	4.4	1.9	0.3	0.3	0.4	20.1
Krt5	Keratin 5	246.8	187.3	622.2	4889.6	1840.6	586.9	742.7	19.8
Exo1	Exonuclease 1	0.2	0.1	0.3	3.4	2.6	0.5	0.6	19.7
Lamc2	Laminin subunit gamma 2	7.5	7.0	56.5	145.8	45.2	11.1	36.3	19.5
Gbx2	Gastrulation brain homeobox 2	0.1	0.1	0.2	1.0	2.1	0.3	1.3	19.4
Sstr4	Somatostatin receptor 4	0.1	0.2	2.3	0.5	0.3	0.4	0.2	19.3

(Continues)

TABLE 8 (Continued)

Gene symbol	Gene name	sFPKM							Expression ratio compared to Unt
		Unt	1 hr	6 hr	1d	3 d	6 d	12 d	
Tmem8c	Transmembrane protein 8C	0.2	0.2	0.1	0.1	0.8	1.7	3.4	18.8
Podnl1	Podocan-like 1	0.2	0.1	0.1	0.2	1.0	2.6	3.0	18.6
Aard	Alanine and arginine rich domain containing protein	0.1	0.2	0.1	0.2	0.5	2.2	2.4	18.5
Il20	Interleukin 20	0.1	0.1	1.0	2.2	0.2	0.1	0.2	18.3
Gjb2	Gap junction protein, beta 2	41.2	21.1	113.2	744.7	305.8	98.1	118.3	18.1
Tgfa	Transforming growth factor alpha	2.9	1.6	23.3	51.9	8.2	4.8	7.2	17.8
Hist1h3a	Histone cluster 1, h3a	0.2	0.2	0.2	2.8	2.4	0.7	0.3	17.7
Ptprv	Protein tyrosine phosphatase, receptor type, V	1.2	0.9	0.8	2.4	16.6	21.2	17.2	17.5
Chrng	Cholinergic receptor nicotinic gamma subunit	0.4	0.5	0.2	0.3	1.7	3.2	6.3	16.6
Spon1	Spondin 1	8.5	8.0	14.6	38.3	110.7	135.2	103.1	15.9
Tuba1c	Tubulin, alpha 1C	0.7	0.9	3.9	10.7	4.1	2.3	4.0	15.9
Lama3	Laminin subunit alpha 3	9.1	7.3	37.9	143.9	42.6	21.3	35.4	15.7
Cenpu	Centromere protein U	0.5	0.5	1.0	8.3	6.3	1.1	1.6	15.6
Rrm2	Ribonucleotide reductase regulatory subunit M2	0.9	0.8	1.6	14.0	10.8	2.1	3.0	15.5
Has3	Hyaluronan synthase 3	1.2	1.2	3.5	18.7	3.6	2.0	3.8	15.5
Adcy8	Adenylate cyclase 8	0.1	0.1	0.1	1.2	1.5	0.2	0.3	15.4
Mybl2	Myeloblastosis oncogene-like 2	0.7	0.6	0.7	10.5	10.3	1.8	2.7	15.2
Cdkn1c	Cyclin-dependent kinase inhibitor 1C	6.9	6.6	3.8	4.2	13.8	103.8	52.6	15.1
Csf2	Colony stimulating factor 2	0.2	0.4	2.9	0.3	0.4	0.3	0.6	15.1
Ccne1	Cyclin E1	0.6	0.5	0.8	8.7	5.7	2.1	1.9	14.7
Nrg1	Neuregulin 1	1.7	1.2	12.2	24.8	5.1	1.7	4.2	14.7
S100vp	S100 calcium-binding protein, ventral prostate	3.4	1.2	0.7	0.4	0.2	48.8	11.4	14.3
Hhipl1	HHIP-like 1	1.2	1.4	0.6	2.6	16.4	14.1	15.0	14.2

Note: Although the actual sFPKM values of measurement had two decimal places, the values were rounded off and expressed using one decimal place in this table. The expression ratio was calculated using the actual values. The actual values are found in Table S1.

Abbreviations: d, day(s); hr, hours; Unt, untreated control.

TABLE 9 Top 50 differentially induced genes in incision-specific secretome

Gene symbol	Gene name	sFPKM							Expression ratio compared to Unt
		Unt	1 hr	6 hr	1 d	3 d	6 d	12 d	
Gip	gastric inhibitory polypeptide	0.1	0.1	0.9	17.5	9.0	0.8	1.2	145.4
Il24	interleukin 24	1.8	3.0	55.7	167.8	10.2	2.6	7.7	91.7
Defb14	defensin beta 14	1.4	0.8	28.3	49.3	19.0	3.1	19.3	36.0
Il19	interleukin 19	0.1	0.1	1.6	2.8	0.4	0.1	0.3	23.7
Avp	arginine vasopressin	0.2	0.2	0.2	0.3	3.9	0.9	0.4	20.7
Camp	cathelicidin antimicrobial peptide	0.2	2.5	4.4	1.9	0.3	0.3	0.4	20.1
Il20	interleukin 20	0.1	0.1	1.0	2.2	0.2	0.1	0.2	18.3
Tgfa	transforming growth factor alpha	2.9	1.6	23.3	51.9	8.2	4.8	7.2	17.8
Csf2	colony stimulating factor 2	0.2	0.4	2.9	0.3	0.4	0.3	0.6	15.1
Lamb3	laminin subunit beta 3	4.0	3.2	26.2	55.3	19.1	8.8	17.7	13.9
Lrg1	leucine-rich alpha-2-glycoprotein 1	12.4	52.9	169.5	31.0	28.1	22.9	21.4	13.7
Emilin1	elastin microfibril interfacer 1	3.9	4.2	3.3	17.2	52.1	29.8	24.2	13.5
Adm2	adrenomedullin 2	0.4	0.2	1.4	4.4	1.8	0.6	0.6	11.6
Il17b	interleukin 17B	2.2	1.7	3.2	24.5	11.6	7.4	7.3	11.0
Scg2	secretogranin II	0.1	0.1	0.1	0.1	0.2	0.6	1.2	10.7
Sfrp2	secreted frizzled-related protein 2	12.0	10.5	13.4	22.4	126.4	107.3	68.1	10.6
Spp2	secreted phosphoprotein 2	0.1	0.1	0.1	0.1	1.2	1.4	1.4	10.2
Tac3	tachykinin 3	0.2	0.4	0.4	0.3	0.9	2.2	2.4	10.2
Il22ra2	interleukin 22 receptor subunit alpha 2	0.1	0.3	1.2	0.3	0.2	0.2	0.2	9.6
Igfbp4	insulin-like growth factor-binding protein 4	55.8	73.1	122.0	295.4	521.0	467.0	425.5	9.3
Aebp1	AE-binding protein 1	39.9	44.1	55.7	64.5	201.4	324.1	263.5	8.1
Serpinb1a	serine (or cysteine) proteinase inhibitor, clade B, member 1a	37.2	42.8	95.7	301.5	160.7	66.4	71.2	8.1
Lum	lumican	193.9	226.7	147.5	282.5	1492.4	1418.4	979.0	7.7
Wnt10a	wingless-type MMTV integration site family, member 10A	0.8	0.7	2.2	5.8	2.0	1.2	1.4	7.3
Erfe	erythroferrone	0.4	0.8	0.5	2.2	2.6	1.1	1.3	6.8
Penk	proenkephalin	1.5	2.9	2.4	1.5	10.1	5.4	8.0	6.7
Serpinb2	serpin family B member 2	55.8	40.5	241.4	363.3	62.1	45.0	62.4	6.5
Wnt4	wingless-type MMTV integration site family, member 4	4.6	3.5	10.3	29.0	8.0	5.7	6.2	6.3
Col27a1	collagen, type XXVII, alpha 1	5.0	4.4	6.6	5.1	27.9	12.0	11.4	5.6
Vstm1	V-set and transmembrane domain containing 1	0.7	2.1	3.6	0.7	0.5	0.6	0.4	5.1

(Continues)

TABLE 9 (Continued)

Gene symbol	Gene name	sFPKM							Expression ratio compared to Unt
		Unt	1 hr	6 hr	1 d	3 d	6 d	12 d	
Arsi	arylsulfatase family, member I	4.4	4.8	5.9	15.9	15.7	10.7	21.7	5.0
Il23a	interleukin 23 subunit alpha	0.5	0.6	1.6	2.5	0.8	0.8	1.0	4.9
Mmp2	matrix metallopeptidase 2	191.2	242.8	186.3	143.3	379.9	912.3	794.5	4.8
Gal	galanin and GMAP prepropeptide	0.3	0.2	0.3	0.2	0.6	0.4	1.4	4.8
Srpx2	sushi-repeat-containing protein, X-linked 2	13.3	12.9	8.2	14.7	53.3	62.3	55.5	4.7
Adamtsl1	ADAMTS-like 1	2.1	3.0	5.1	3.0	5.9	9.4	5.9	4.4
Ptn	pleiotrophin	22.9	20.0	16.7	21.6	84.9	99.2	69.8	4.3
Vwa1	von Willebrand factor A domain containing 1	9.6	9.5	12.7	40.5	33.4	18.9	22.9	4.2
Mmp23	matrix metallopeptidase 23	8.7	9.9	6.7	5.2	22.2	35.5	28.7	4.1
Igfbp3	insulin-like growth factor-binding protein 3	10.5	10.4	16.6	42.6	32.4	24.2	34.3	4.1
Adamts7	ADAM metallopeptidase with thrombospondin type 1 motif, 7	2.5	2.3	3.3	3.0	6.5	10.2	9.1	4.0
Plod3	procollagen-lysine, 2-oxoglutarate 5-dioxygenase 3	11.6	13.1	23.6	23.5	45.3	25.0	25.5	3.9
Ndnf	neuron-derived neurotrophic factor	0.4	0.5	0.2	0.4	1.1	1.5	0.8	3.8
Anxa2	annexin A2	676.3	650.2	1353.9	2549.0	1571.8	914.5	1390.4	3.8
Cxcl12	C-X-C motif chemokine ligand 12	24.6	22.0	23.0	23.9	42.3	91.2	76.7	3.7
Pgf	placental growth factor	4.0	4.8	5.9	9.3	14.1	6.3	10.3	3.5
Hamp	hepcidin antimicrobial peptide	0.6	0.3	2.0	0.3	0.2	0.3	0.2	3.4
Igf2	insulin-like growth factor 2	19.2	16.7	12.5	5.4	9.2	41.4	64.8	3.4
Il34	interleukin 34	3.4	3.3	2.6	2.5	3.8	11.5	7.8	3.4
Wisp2	WNT1 inducible signaling pathway protein 2	58.4	72.2	19.0	72.1	106.9	189.9	121.9	3.3

Note: Although the actual sFPKM values of measurement had two decimal places, the values were rounded off and expressed using one decimal place in this table. The expression ratio was calculated using the actual values. The actual values are found in Table S1.

Abbreviations: d, day(s); hr, hours; Unt, untreated control.

and (3) tissue repair as the wound closes completely. Interspersed through all the phases are alterations in lipid biosynthesis and signaling processes which are discussed. However, not all changes reported can be discussed in detail and more connections can be made over both time and gene families using these data as a discovery resource.

4.1 | Initial phase of wound healing process (1 hour to 1 day after incising)

Tissue invasion by surgical incision was characterized by rapidly developing hyperalgesic behavioral changes, and macro and microscopic tissue changes. Hind paw edema commenced from 1 hour after incising and was prolonged through 12 days after incising (Figure 1A). The early elevation, especially the rapid and high expression of *Cxcl1*, *Cxcl2*, *Il1b*, and *Il6* after incising (Figure 1H), is consistent with the idea that resident immune cells quickly express and secrete these neutrophil chemoattractants to recruit circulating leukocytes into the damaged site, and then the recruited immune cells express additional inflammatory cytokines to further enhance the inflammatory response.[26,36] The recruitment of leukocytes was confirmed by the histological findings shown in Figure 1E and increases of the mRNAs for the neutrophil markers *S100a8* and *S100a9* at 1 day after incising (Figure 1H). These results illustrate that neutrophils are rapidly recruited as shown in a previous study,[37] and their infiltration reached a peak at 1 day after incising in response to *Cxcl1* and *Cxcl2*. These findings were also seen in the peripheral inflammation model (Figure 7D). Neutrophils are thought to be major sources of inflammatory molecules that also function as algesic factors, which suggests that neutrophil recruitment contributes to the observed hyperalgesia and allodynia.[38] However, one study showed that neutrophil depletion did not reduce these algesic endpoints in the surgical incision model in mice.[39] In addition to inflammation enhancing responses, an anti-inflammatory cytokine, *Il10*, was also upregulated (Figure 1H). By inhibiting NF-kappa B activity, IL10 counteracts inflammatory responses.[40] These transcriptional alterations, that have seemingly conflicting roles with each other, may orchestrate various aspects of the complex inflammatory response in incised tissue.[41] This type of opponent process occurs frequently across multiple gene functions such as proteases and protease inhibitors and likely represent dynamic processes to preserve physiological homeostasis and tissue integrity.

The S100A8/A9 proteins form a calcium-binding dimeric complex, which is recognized by Toll-like receptor 4 and is known as a damage-associated molecular pattern.[42] These proteins may have a role in the terminal differentiation of keratinocytes as the keratinocytes undergo expulsion of the nucleus to form the cornified epithelium. Recently, it has been reported that S100A8/A9 have important roles in tissue repair. S100A9 knock out mice, which are deficient for the complex, displayed increased tissue damage, sustained inflammation, induction of fibrosis, and increased expression of collagens following ischemia/reperfusion-induced injury of renal tissue compared with wild-type mice.[43] Injection of mesenchymal stem cells treated with S100A8/A9 accelerated wound healing in a full-thickness cutaneous wound model in mice.[44] On the other hand, another study also used S100A9 knock-out mice and showed decreased migration rates of neutrophils but accelerated wound healing compared with wild-type mice.[45] While the types and locations of tissue injuries may affect the behavior of S100A8/A9 for repair, our data, that represent normal primary intentional wound healing processes, showed wound closure and collagen synthesis following the upregulation of *S100a8* and *S100a9*. We found that, in addition to the expression of *S100a9* in leukocytes in the dermal layer, *S100a9* was expressed in epidermally located keratinocytes at 6 hours and 1 day after incising, when a thickened epidermal layer was observed. Epidermal keratinocytes are known to have a key role in skin tissue repair. This is consistent with a previously reported result that S100A8 and S100A9 protein levels were increased in hypertrophic scars in humans.[46] This study also showed that knock down of either gene suppressed migration of keratinocytes, that both proteins were associated with activation of fibroblasts, and that the expression of both genes was downregulated by knock down of cyclooxygenase 2 (*Ptgs2*) (see below).

Classically, prostanoids, which are synthesized by the action of cyclooxygenases on arachidonic acid (AA) followed by further actions of prostaglandin and thromboxane synthases,[47] have been shown to mediate pain and inflammation.[48] In our dataset, *Ptgs2* was sharply upregulated prior to the upregulation of *S100a8* and *S100a9* (Figure 4C). These sequential observations suggest that cyclooxygenase 2 (COX2) is necessary to initiate and maintain wound healing process associated with S100A8 and S100A9, and that NSAIDs which inhibit COX1 and 2 possibly negatively affect wound healing as reported previously.[49,50] We found a strikingly consistent expression pattern among transcripts encoding enzymes that synthesize prostanoids (Figure 5B,C), with expression of all but one of these transcripts being elevated from baseline at 6-hours post-incision indicating that these genes are induced locally as opposed to being imported from infiltrating immune cells. Taken together, the present data suggest that S100A8 and S100A9 are key regulators of wound healing process in skin, and the sequential

expression of *Ptgs2* followed by *S100a8*, and *S100a9* is important for regulation of inflammation and pain because the protein complex formed by S100A8 and S100A9 is involved in AA metabolism.[51] Additionally, specific ALOX enzymes convert AA and docosahexaenoic acid (DHA) to eicosanoids and SPMs, respectively, which have been demonstrated to play a role in inflammation as well as the resolution of inflammation.[52] We determined several lipoxygenase-encoding transcripts that were constantly expressed over the time course examined. It has been proposed that linoleic acid (LA) bound to ceramide EOS (Ester-linked Omega hydroxy FA) + S (sphingosine) gets converted, by the subsequent action of arachidonate 12-lipoxygenase, 12R type (*Alox12b*) and arachidonate lipoxygenase 3 (*Aloxe3*), to an epoxy-alcohol LA derivative.[33] This ceramide bound LA-epoxy-alcohol can then be hydrolyzed to form OS[30] or converted by the action of short chain dehydrogenase/reductase family 9C member 7 (*Sdr9c7*) to an epoxy-ketone LA derivative (which can also be hydrolyzed to form OS).[53] OS or ceramide OS bound epoxy-ketone LA derivatives can then be covalently bound to the corneocyte envelope to form the cornified lipid envelope.[53] Interestingly, we found the temporal expression patterns of *Alox12b* and *Aloxe3* were similar and remained generally unchanged, while the short-chain dehydrogenase/reductase family member *Sdr9c7* initially decreased, subsequently underwent upregulation beginning at 6 hours which was sustained for the 12 day observation period as the wound closed (Figure 5B,C). This pattern suggests this gene, which causes autosomal recessive congenital ichthyosis, plays an important role in wound healing. Taken together the temporal pattern of gene expression is consistent with a concerted mobilization of gene regulatory pathways to promote wound healing and repair of the epidermal cornified lipid envelope.

As discussed earlier, neutrophil infiltration started in this phase in response to neutrophil chemoattractants, which were secreted probably by resident immune cells such as monocytes and macrophages. This idea is supported by Imsig analysis (Figure 6A,B). The second peak of the monocytes and macrophages may indicate further infiltration of these cell types in addition to the activation of the resident cells. Imsig analysis also showed a comparatively smaller molecular signature consistent with T cell activation at 6 hours after incision. For wound healing, resident γδ T cells in both epidermis and dermis play important roles through interaction with damaged keratinocytes.[54] Once they recognize damage in keratinocytes, they gather within 24 hours after wounding. Detailed functions of these immune cells and the T cell activation can be further investigated using single-cell RNA-seq analysis.

4.2 | Middle phase of wound healing process (1 day to 3 days after incising)

Importantly, thermal hyperalgesia and mechanical allodynia were most severe at 1 day after incising (Figure 1B-D), when aggregation of immune cells, especially neutrophils (Figures 1E, 6A, and 5B), thickening of the epidermal layer (Figures 1E and 3A), and an increased number of transcripts were observed in both the whole gene dataset (Figure 1F) and the incision-specific gene set as well (Figure 8A). Prior to the behavioral changes, transcripts related to sensory perception of pain were most actively upregulated at 6 hours after incising (Figure 4A). These genes include two chemokines and an interleukin, a neurotrophic factor, and several receptors. CCL2 and CCL3 which are encoded by *Ccl2* and *Ccl3*, respectively, have been reported to contribute to enhancing nociceptive behaviors peripherally.[55,56] *Ptgs2* showed sustained expression from 1 hour to 1 day after incising (Figure 4C,E). These results suggest early involvement of prostaglandins in initiating the post-incisional hyperalgesia which may be sustained for more than a day and further enhancement or maintenance of the hyperalgesia by CCL2 and CCL3. These sequential expressions were also observed in carrageenan inflamed hind paw where the expression of *Ptgs2* was induced by 1 hour but returned to the baseline by 4 hours.[16,57] In contrast, with incision, we observed a sustained expression pattern of *Ptgs2* which may be consistent with multiple cell sources for the gene, multiple triggers for the induction(s), and sustained expression to further augment inflammation and hyperalgesia. Interestingly, transcripts for almost all known prostanoid and eicosanoid receptors increased from baseline as a result of incision (Figure 5B). For most of these receptors, peak expression occurred by 1 day after incision. The transcript for *Ptger2* exhibited the largest change in expression (34-fold increase) that peaked at 6 hours and returned to baseline over the remainder of the time course (Figure 5C), consistent with the reported enrichment of this transcript in T-cells (Figure 6A). Together these results indicate that prostaglandin and leukotriene signaling is elevated after incision and this elevation is due to a combination of immune cell infiltration and local induction, implying a role for oxylipins in mediating the wound healing response in a multifactorial fashion. We also observed upregulation of *Ednrb* encoding endothelin receptor type B (ET$_B$) at 6 hours after incising. It is known to be locally involved in stimulating nociceptive behavior and its ligand, endothelin, may modulate neuronal purinergic receptor sensitization during inflammatory/tissue damage pain, especially P2X4 encoded by *P2rx4*

which was upregulated in the later phase.[58,59] These gene expression changes are also quite similar to those observed in the inflammation model.[16] The results suggest that the biological responses to surgical incision, particularly related to inflammation and pain generation, were rapidly initiated by *Ptgs2* whose expression was enhanced through 6 hours to 1 day after incising, coincident with the peak of nociception.

Genes encoding ALOX enzymes involved in eicosanoid and SPMs exhibited a more nuanced expression pattern in the middle phase of the wound healing process. Expression of *Alox12,* which encodes an enzyme that synthesizes 12-hydroxyeicosatetraenoic acid and maresins (from AA and DHA, respectively) that have been demonstrated to play a role in inflammation[60] and resolution of inflammation,[61] respectively, peaked at 1 day post-incision, consistent the enrichment of this gene in neutrophils (https://www.proteinatlas.org/ENSG00000108839 -ALOX12/blood, v20.1.proteinatlas.org).[62] This is supported by the expression pattern of neutrophils shown by the Imsig analysis (Figure 6A). Conversely, expression of *Alox5* and *Alox15,* which encode enzymes that convert AA into proinflammatory leukotrienes or pro-resolving lipoxins and DHA into resolvins and protectins (SPMs) tended to decrease after incision. In the peripheral carrageenan inflammation model, *Alox5* showed a time-dependent increase in expression, and *Alox15* was temporarily upregulated at 1 day after inflammation induction.[57] A significant reduction of the two transcript levels was observed at 1 day after incising in the incision model. The decrease in expression of these enzymes, despite the infiltration of immune cells reported to express these genes[63] is consistent with the idea that these genes are being downregulated within the immune cell population. In addition, the difference in expression patterns compared with the inflammation model leads to us to hypothesize that the suppression of these lipoxygenases after incising plays a modality-specific role to promote tissue repair and regeneration through regulation of the inflammatory response in the incised tissue.

At the 24-hour time, *Nppb*, which encodes brain natriuretic peptide B (BNP), was detected as the most DEG (Figure 2C). It had the highest expression ratio among all of the DEGs (Table S1) and revealed an expression pattern (and level) that was distinguishable from the expression pattern in the inflammation model (Figure 7F). As revealed by in situ hybridization, *Nppb* was located around wound edges in the epidermal layer, and its receptors, *Npr1* and *Npr3,* were located broadly in skin tissue (Figure 7G). An involvement of *Nppb* in skin pathophysiology is suggested by studies in patients with atopic dermatitis, where protein expression of BNP and its receptor, NPR1 was increased in the epidermal layer.[64] In terms of wound healing, it has been reported that intradermal injection of BNP possibly reduced scar formation in a full-thickness cutaneous wound model in rats.[65] Recently, a contribution of *Nppb* (BNP) to induction of itching in both central and peripheral nerves was reported, but possible functions of *Nppb* (BNP) in skin were not reported.[64,66,67] A role for central BNP in pain is suggested by the observation that intrathecal injection of BNP can suppress inflammatory pain induced in rat hind paw.[68,69] These mouse primary afferent neuron studies suggest a role in sensory transduction but this is very distinct from the regulated expression we see in skin. Additionally, the expression of BNP in rat DRG is substantially lower than in mouse.[70] Therefore, the findings related to the expression changes of *Nppb*, *Npr1*, and *Npr3* in our skin incision dataset indicate biological roles in the wound healing process that are distinct from sensory functions in peripheral neurons. Further studies targeting specific roles of these genes and their encoding peptides or receptors are required to ascertain the exact functions on *Nppb* (BNP) and its receptors in damaged skin.

In this phase, we found some important cell types for nociception and wound healing, which can be further investigated with the sequencing of single-cell preparations in addition to the cellular level anatomical localization done with in situ hybridization and standard histology. Neutrophil accumulation was significant as shown histologically and by Imsig analysis. In addition, epidermal thickening and collagen synthesis were also histologically observed, which was consistent with the upregulation of proliferation signaling (Figure 6C,D). Epidermal cells such as keratinocytes, which are probably the sources of *Nppb* and dermal cells including fibroblasts and vascular endothelial cells, which expressed *Npr1* and *Npr3* (Figure 7G) may be related to the phenomena observed. Previous studies reported that BNP which activates cGMP-dependent signaling had important roles in keratinocyte and endothelial cells through NPR1,[71,72] which may have roles in keratinocyte migration and angiogenesis during wound healing respectively.[73,74] This suggests a new hypothesis that BNP may contribute to wound healing by promoting keratinocyte migration and stimulation of endothelial cells for angiogenesis via a BNP/NPR1 pathway.

4.3 | Late phase of wound healing process (3 days to 12 days after incising)

We extended the time course out to 12 days to assess completion of the wound-healing process and other biological responses following surgical incision. However, closure of the incision and infiltration of immune cells occurred between 6 hours and 1 day after incising (Figures 1E

and 3A) when 24 out of the top 30 transcripts known to be related to wound healing had their peak expression (Figure 3D). Interestingly, *Il24*, *Tgfa*, and *Nrg1* were also detected as incision-model-specific genes (Figure 8C). In particular, it was reported that *Nrg1* was involved in Schwann cell development and myelination.[75] and the protein product, neuregulin1 is a ligand for epidermal growth factor receptor, *Erbb3*. These genes are possible candidates for new therapeutic targets related to epithelial or nerve specific repair processes and may be potential wound healing biomarkers for traumatic injuries that involve peripheral nerve damage.

From the incisional secretome analysis, we found upregulation of several members of the matrix metalloproteinases (MMPs) family, *Mmp9*, *Mmp12*, and *Mmp13* at 1 day after incising, and *Mmp9* and *Mmp12* showed prolonged expression (Figure 2D). MMPs are known to degrade collagen tissues and have important roles in wound healing, and they are classified into groups such as: *Mmp9*, gelatinases; *Mmp12*, macrophage metalloelastase; and *Mmp13*, interstitial collagenases.[76] MMP9-knock-out mice showed impaired neovascularization in the wound area, increased inflammation, decreased collagen deposition, and decreased peripheral blood endothelial progenitor cells,[77] which may delay wound healing. On the other hand, wound exudate obtained from chronic leg ulcers contained elevated level of MMP9.[78] Our data also showed that the tissue inhibitor of metalloproteinases 1, *Timp1*, was upregulated through 6 hours to 3 days after incising (Figure 3D), indicating a balanced regulation of tissue degradation and remodeling. A failure in the regulation of this system possibly triggers chronification of the incisional wound. Thus, interventions to this system represent potential candidate therapeutic strategies. In addition to proteolysis of a number of proteins, it is known that MMP12 is mainly expressed in macrophages and is required for their migration.[79,80] The expression pattern of *Mmp12* in our dataset is consistent with the temporal pattern of macrophage activity in the incised tissue and is supported by the Imsig analysis (Figure 6A,B). It was reported that MMP13 knock-out mice displayed delayed epithelialization, possibly by impaired migration of keratinocytes and lower vascular density in wound granulation in a full-thickness wound model in mice.[81] The histological analyses in this study showed that the wound closure was almost completed during 1 to 3 days after incising (Figures 1E and 3A), which was consistent with the sharp expression peak of *Mmp13* at 1 day after incising (Figure 2D).

Analyzing the incisional secretome showed that the greatest number of regulated genes encoding secreted proteins occurred at 6 days after incising although the expression ratios of the genes at this time point were relatively low

(the maximum expression ratio was 16.8 for *Cthrc1*, coding for collagen triple helix repeat containing 1) (Figure 2C). When the incision had closed (6 days), infiltrated immune cells were still clearly observed in the tissue. We found five peptidase encoding genes that had their peak expression at 6 days after incising in the incision specific category of DEGs, *Mmp2*, *Aebp1*, *Mmp23*, *Adamts7*, and *Adamtsl1* (Figure 8D). One previous study reported that mice lacking aortic carboxypeptidase-like protein, which is an alias of *Aebp1*, led to deficient wound healing.[82] The temporal expression change of *Mmp2* was consistent with previously reported expression pattern for the protein level, in which macrophages were the source of MMP2.[83] However, the expression level of *Mmp2* in the present study is quite high even at baseline (191.2 sFPKM at baseline and 912.3 sFPKM at 6 days after incising), which may indicate the transcript is produced in local cells, and macrophages bring in even more. MMP2 has important roles in wound healing, but excessive activation in the acute phase leads to impaired wound healing.[84,85] In chronic wounds, an impaired ability of fibroblasts to reorganize extracellular matrix in vitro is related to decreased levels of active matrix metalloproteinase-2.[86] In contrast, association of *Mmp23*, *Adamts7*, and *Adamtsl1* with wound healing has not been reported. Taken together, we propose a new hypothesis that misregulation of the peptidases detected from our dataset may be associated with the chronification of wounds, and these molecules may serve as wound healing biomarkers and, potentially, new preventive therapeutic targets for chronic wounds.

At this late phase, both thermal hyperalgesia and mechanical allodynia were resolving (Figure 1B-D). At 3 days after incising, we detected *Penk* transcripts which encode the proenkephalin precursor protein that is proteolytically processed to produce the endogenous opioid pentapeptides, Met5- and Leu5-enkephalin and the C-terminally extended octapeptide and heptapeptide.[87-89] It is reported that *Penk* was upregulated in rat dorsal horn during peripheral inflammation in hind paw suggesting a function in pain regulation in the central nervous system.[90] In peripheral tissue, a previous study reported that proenkephalin was expressed in human skin and cultured cells, especially in keratinocytes and fibroblasts at both the transcript and protein levels. The expression was upregulated by stimulation with ultraviolet radiation and agonists of toll-like receptor 4 and 2.[91] It is also reported that proenkephalin positive regulatory T cells were involved with wound healing.[92] According to the Imsig analysis, T cell had a second peak at 3 days after incising (Figure 6A,B), which was consistent with the upregulation of *Penk*. These suggest that the recruited regulatory T cell and *Penk* have roles in the incision. The source of *Penk* should be observed as single cell level with deeper analysis for their

functions. While contributions of *Penk* to peripheral tissue are still understudied, it may have important roles in both wound healing and wound pain regulation through opioid receptors expressed in skin cells such as keratinocytes. We also detected *P2rx4* upregulation, which encodes purinergic receptor P2X4. Through ATP-P2X4 signaling, epidermal keratinocytes act as sensors for mechanical, thermal, and cold nociceptive stimuli.[59,93,94] This upregulation of *P2rx4* may increase sensitivity of the skin tissue around the incised area to prevent the tissue from undergoing secondary damage during the remodeling phase thereby contributing to recovery from incision.

As shown in Figure 1E, there were still abundant infiltrated immune cells. Imsig analysis suggested they were mainly monocytes and macrophages (Figure 6A,B). It is well known that macrophages have important roles in wound healing and are a source of peptidase families, while dysregulation of macrophage activities and over expression of peptidases lead the chronification of wounds.[78,95] To analyze the functions of the cells in this phase may be able to clarify mechanisms of chronification of wounds.

5 | CONCLUSION

The present study profiled temporal transcriptomic regulation in the surgical incision model from several aspects: temporal expression changes, subcellular localizations, wound healing, sensory perception of pain, oxylipin synthesis, immune cell activities, and comparison with peripheral inflammation. Several candidates for biomarkers or new therapeutics, CXCL1, CXCL2, S100A8/A9, and NPPB (BNP), were identified. One limitation to full interpretation of the results in the present study is the lack of data from female rats to assess the effect of sex on the biological reactions to the surgical incision. While a previous study showed similar post-operative pain and analgesic response between male and female rats using the incision model,[96] sex may influence the immune responses, and also pain perception in central nervous system regions.[97,98] In this study, however, we aimed to simplify the analyses to show other complex alterations in gene expressions such as temporal alterations and comparison with the inflammation model. A separate study will address the issue of sex specificity. Another limitation is that we did not show the expressions of target molecules translated into protein/peptide levels. While this study concentrates on mRNA levels and regulation of gene expression, there is evidence that the gene changes measured can result in altered levels of their products. For example, the infiltration of neutrophils occurred as a consequence of *Cxcl1* and *Cxcl2* upregulations which is consistent with the idea that these transcripts were translated and used as neutrophil chemoattractants. The major alterations of transcripts we observed, especially of the many chemokines and proinflammatory cytokines, were consistent with the accumulated evidence from previous protein-based studies, reinforcing the idea that many of the transcripts we detected were translated and used.

Our results provide foundational knowledge to understand molecular dynamics during the injury and healing process of the surgical incision and incision-induced hyperalgesic states that may inform the post-surgical wound status of a patient which, in turn, can help guide clinical decisions.

CONFLICT OF INTEREST
None of the authors declare a conflict of interest.

AUTHOR CONTRIBUTIONS
TG designed and performed animal surgery, performed behavioral testing on the animals, RNA-Seq analyses, in situ hybridization, interpreted the data, constructed figures and wrote the paper. MRS designed experiments, performed RNA-Seq analyses, statistics, and analyzed and interpreted the data. DM supervised image acquisition and figure construction. JMR performed bioinformatic analyses, constructed figures and interpreted data. AFD performed RNA-Seq analyses and analyzed and interpreted the data. LNS interpreted the data and supervised writing the paper. AJM interpreted the data and supervised writing the paper. MJI designed experiments, supervised research, supervised figure construction and data interpretation and worked on writing the paper.

ORCID
Taichi Goto https://orcid.org/0000-0001-7140-8175
Matthew R. Sapio https://orcid.org/0000-0002-8855-5419
Dragan Maric https://orcid.org/0000-0003-2912-7921
Jeffrey M. Robinson https://orcid.org/0000-0002-1456-2851

Anthony F. Domenichiello https://orcid.
org/0000-0003-4808-8403
Leorey N. Saligan https://orcid.
org/0000-0001-9481-7836
Andrew J. Mannes https://orcid.
org/0000-0001-5834-5667
Michael J. Iadarola https://orcid.
org/0000-0001-7188-9810

REFERENCES

1. Nussbaum SR, Carter MJ, Fife CE, et al. An economic evaluation of the impact, cost, and medicare policy implications of chronic nonhealing wounds. *Value Health*. 2018;21(1):27-32.
2. Gan TJ, Habib AS, Miller TE, White W, Apfelbaum JL. Incidence, patient satisfaction, and perceptions of post-surgical pain: results from a US national survey. *Curr Med Res Opin*. 2014;30(1):149-160.
3. Joshi GP, Rawal N, Kehlet H, et al. Evidence-based management of postoperative pain in adults undergoing open inguinal hernia surgery. *Br J Surg*. 2012;99(2):168-185.
4. Roberts M, Brodribb W, Mitchell G. Reducing the pain: a systematic review of postdischarge analgesia following elective orthopedic surgery. *Pain Med*. 2012;13(5):711-727.
5. Wunsch H, Wijeysundera DN, Passarella MA, Neuman MD. Opioids prescribed after low-risk surgical procedures in the United States, 2004–2012. *JAMA*. 2016;315(15):1654-1657.
6. Fivenson DP, Faria DT, Nickoloff BJ, et al. Chemokine and inflammatory cytokine changes during chronic wound healing. *Wound Repair Regen*. 1997;5(4):310-322.
7. Goto T, Tamai N, Nakagami G, et al. Can wound exudate from venous leg ulcers measure wound pain status?: a pilot study. *PLoS One*. 2016;11(12):e0167478.
8. Ebrecht M, Hextall J, Kirtley LG, Taylor A, Dyson M, Weinman J. Perceived stress and cortisol levels predict speed of wound healing in healthy male adults. *Psychoneuroendocrinology*. 2004;29(6):798-809.
9. McGuire L, Heffner K, Glaser R, et al. Pain and wound healing in surgical patients. *Ann Behav Med*. 2006;31(2):165-172.
10. Brennan TJ, Vandermeulen EP, Gebhart GF. Characterization of a rat model of incisional pain. *Pain*. 1996;64(3):493-501.
11. Raithel SJ, Sapio MR, LaPaglia DM, Iadarola MJ, Mannes AJ. Transcriptional changes in dorsal spinal cord persist after surgical incision despite preemptive analgesia with peripheral resiniferatoxin. *Anesthesiology*. 2018;128(3):620-635.
12. Tran PV, Johns ME, McAdams B, Abrahante JE, Simone DA, Banik RK. Global transcriptome analysis of rat dorsal root ganglia to identify molecular pathways involved in incisional pain. *Mol Pain*. 2020;16:1744806920956480.
13. Winter CA, Risley EA, Nuss GW. Carrageenin-induced edema in hind paw of the rat as an assay for antiiflammatory drugs. *Proc Soc Exp Biol Med*. 1962;111:544-547.
14. Watanabe M, Ueda T, Shibata Y, Kumamoto N, Ugawa S. The role of TRPV1 channels in carrageenan-induced mechanical hyperalgesia in mice. *NeuroReport*. 2015;26(3):173-178.
15. Hargreaves K, Dubner R, Brown F, Flores C, Joris J. A new and sensitive method for measuring thermal nociception in cutaneous hyperalgesia. *Pain*. 1988;32(1):77-88.
16. Goto T, Sapio MR, Maric D, et al. Longitudinal transcriptomic profiling in carrageenan-induced rat hind paw peripheral inflammation and hyperalgesia reveals progressive recruitment of innate immune system components. *J Pain*. 2020;22(3):322-343.
17. Alexandre C, Latremoliere A, Ferreira A, et al. Decreased alertness due to sleep loss increases pain sensitivity in mice. *Nat Med*. 2017;23(6):768-774.
18. LaPaglia DM, Sapio MR, Burbelo PD, et al. RNA-Seq investigations of human post-mortem trigeminal ganglia. *Cephalalgia*. 2018;38(5):912-932.
19. Zhang W, Yu Y, Hertwig F, et al. Comparison of RNA-seq and microarray-based models for clinical endpoint prediction. *Genome Biol*. 2015;16:133.
20. The UniProt Consortium. UniProt: the universal protein knowledgebase. *Nucleic Acids Res*. 2018;46(5):2699.
21. Rastogi S, Rost B. LocDB: experimental annotations of localization for Homo sapiens and *Arabidopsis thaliana*. *Nucleic Acids Res*. 2011;39(suppl_1):D230-D234.
22. Binder JX, Pletscher-Frankild S, Tsafou K, etal. COMPARTMENTS: unification and visualization of protein subcellular localization evidence. *Database (Oxford)*. 2014;2014:bau012.
23. Thul PJ, Åkesson L, Wiking M, et al. A subcellular map of the human proteome. *Science*. 2017;356(6340):eaal3321.
24. Smith JR, Hayman GT, Wang S-J, et al. The Year of the Rat: the Rat Genome Database at 20: a multi-species knowledgebase and analysis platform. *Nucleic Acids Res*. 2020;48(D1):D731-D742.
25. Nirmal AJ, Regan T, Shih BB, Hume DA, Sims AH, Freeman TC. Immune cell gene signatures for profiling the microenvironment of solid tumors. *Cancer Immunol Res*. 2018;6(11):1388-1400.
26. De Filippo K, Dudeck A, Hasenberg M, et al. Mast cell and macrophage chemokines CXCL1/CXCL2 control the early stage of neutrophil recruitment during tissue inflammation. *Blood*. 2013;121(24):4930-4937.
27. Wang S, Song R, Wang Z, Jing Z, Wang S, Ma J. S100A8/A9 in inflammation. *Front Immunol*. 2018;9:1298.
28. Chiba T, Thomas CP, Calcutt MW, Boeglin WE, O'Donnell VB, Brash AR. The precise structures and stereochemistry of trihydroxy-linoleates esterified in human and porcine epidermis and their significance in skin barrier function: implication of an epoxide hydrolase in the transformations of linoleate. *J Biol Chem*. 2016;291(28):14540-14554.
29. Munoz-Garcia A, Thomas CP, Keeney DS, Zheng Y, Brash AR. The importance of the lipoxygenase-hepoxilin pathway in the mammalian epidermal barrier. *Biochim Biophys Acta*. 2014;1841(3):401-408.
30. Zheng Y, Yin H, Boeglin WE, et al. Lipoxygenases mediate the effect of essential fatty acid in skin barrier formation: a proposed role in releasing omega-hydroxyceramide for construction of the corneocyte lipid envelope. *J Biol Chem*. 2011;286(27):24046-24056.
31. Dalli J, Vlasakov I, Riley IR, et al. Maresin conjugates in tissue regeneration biosynthesis enzymes in human macrophages. *Proc Natl Acad Sci U S A*. 2016;113(43):12232-12237.
32. Samuelsson B. Role of basic science in the development of new medicines: examples from the eicosanoid field. *J Biol Chem*. 2012;287(13):10070-10080.
33. Serhan CN. Pro-resolving lipid mediators are leads for resolution physiology. *Nature*. 2014;510(7503):92-101.

34. Serhan CN, Levy BD. Resolvins in inflammation: emergence of the pro-resolving superfamily of mediators. *J Clin Invest*. 2018;128(7):2657-2669.

35. Spofford CM, Brennan TJ. Gene expression in skin, muscle, and dorsal root ganglion after plantar incision in the rat. *Anesthesiology*. 2012;117(1):161-172.

36. Rose-John S. Interleukin-6 family cytokines. *Cold Spring Harb Perspect Biol*. 2018;10(2):a028415.

37. Peters NC, Egen JG, Secundino N, et al. In vivo imaging reveals an essential role for neutrophils in leishmaniasis transmitted by sand flies. *Science*. 2008;321(5891):970-974.

38. Carreira EU, Carregaro V, Teixeira MM, et al. Neutrophils recruited by CXCR1/2 signalling mediate post-incisional pain. *Eur J Pain*. 2013;17(5):654-663.

39. Sahbaie P, Li X, Shi X, Clark JD. Roles of Gr-1+ leukocytes in postincisional nociceptive sensitization and inflammation. *Anesthesiology*. 2012;117(3):602-612.

40. Wang P, Wu P, Siegel MI, Egan RW, Billah MM. Interleukin (IL)-10 inhibits nuclear factor kappa B (NF kappa B) activation in human monocytes. IL-10 and IL-4 suppress cytokine synthesis by different mechanisms. *J Biol Chem*. 1995;270(16):9558-9563.

41. Lewis GP. *Mediators of Inflammation*. Oxford: Wright; 1986.

42. Ehrchen JM, Sunderkotter C, Foell D, Vogl T, Roth J. The endogenous Toll-like receptor 4 agonist S100A8/S100A9 (calprotectin) as innate amplifier of infection, autoimmunity, and cancer. *J Leukoc Biol*. 2009;86(3):557-566.

43. Dessing MC, Tammaro A, Pulskens WP, et al. The calciumbinding protein complex S100A8/A9 has a crucial role in controlling macrophage-mediated renal repair following ischemia/reperfusion. *Kidney Int*. 2015;87(1):85-94.

44. Basu A, Munir S, Mulaw MA, et al. A novel S100A8/A9 induced fingerprint of mesenchymal stem cells associated with enhanced wound healing. *Sci Rep*. 2018;8(1):6205.

45. Vogl T, Ludwig S, Goebeler M, et al. MRP8 and MRP14 control microtubule reorganization during transendothelial migration of phagocytes. *Blood*. 2004;104(13):4260-4268.

46. Zhong A, Xu W, Zhao J, et al. S100A8 and S100A9 are induced by decreased hydration in the epidermis and promote fibroblast activation and fibrosis in the dermis. *Am J Pathol*. 2016;186(1):109-122.

47. Vane JR, Bakhle YS, Botting RM. Cyclooxygenases 1 and 2. *Annu Rev Pharmacol Toxicol*. 1998;38:97-120.

48. Vane JR, Botting RM. The mechanism of action of aspirin. *Thromb Res*. 2003;110(5-6):255-258.

49. Goto T, Nakagami G, Minematsu T, Shinoda M, Sanada H. Measurement of mechanical withdrawal threshold on full-thickness cutaneous wounds in rats using the von Frey test. *J Wound Care*. 2019;28(11):762-772.

50. Schug SA. Do NSAIDs really interfere with healing after surgery? *J Clin Med*. 2021;10(11):2359.

51. Kerkhoff C, Klempt M, Kaever V, Sorg C. The two calciumbinding proteins, S100A8 and S100A9, are involved in the metabolism of arachidonic acid in human neutrophils. *J Biol Chem*. 1999;274(46):32672-32679.

52. Serhan CN, Chiang N, Dalli J. The resolution code of acute inflammation: novel pro-resolving lipid mediators in resolution. *Semin Immunol*. 2015;27(3):200-215.

53. Takeichi T, Hirabayashi T, Miyasaka Y, et al. SDR9C7 catalyzes critical dehydrogenation of acylceramides for skin barrier formation. *J Clin Invest*. 2020;130(2):890-903.

54. Munoz LD, Sweeney MJ, Jameson JM. Skin resident gammadelta T cell function and regulation in wound repair. *Int J Mol Sci*. 2020;21(23):9286.

55. Llorián-Salvador M, González-Rodríguez S, Lastra A, et al. Involvement of CC chemokine receptor 1 and CCL3 in acute and chronic inflammatory pain in mice. *Basic Clin Pharmacol Toxicol*. 2016;119(1):32-40.

56. Luo P, Shao J, Jiao Y, Yu W, Rong W. CC chemokine ligand 2 (CCL2) enhances TTX-sensitive sodium channel activity of primary afferent neurons in the complete Freud adjuvant-induced inflammatory pain model. *Acta Biochim Biophys Sin (Shanghai)*. 2018;50(12):1219-1226.

57. Domenichiello AF, Sapio MR, Loydpierson AJ, et al. Molecular pathways linking oxylipins to nociception in rats. *J Pain*. 2021;22(3):275-299.

58. Khodorova A, Fareed MU, Gokin A, Strichartz GR, Davar G. Local injection of a selective endothelin-B receptor agonist inhibits endothelin-1-induced pain-like behavior and excitation of nociceptors in a naloxone-sensitive manner. *J Neurosci*. 2002;22(17):7788-7796.

59. Barr TP, Hrnjic A, Khodorova A, Sprague JM, Strichartz GR. Sensitization of cutaneous neuronal purinergic receptors contributes to endothelin-1-induced mechanical hypersensitivity. *Pain*. 2014;155(6):1091-1101.

60. Zhang X-J, Cheng XU, Yan Z-Z, et al. An ALOX12-12-HETE-GPR31 signaling axis is a key mediator of hepatic ischemia-reperfusion injury. *Nat Med*. 2018;24(1):73-83.

61. Serhan CN, Chiang N, Dalli J. New pro-resolving n-3 mediators bridge resolution of infectious inflammation to tissue regeneration. *Mol Aspects Med*. 2018;64:1-17.

62. Uhlen M, Fagerberg L, Hallstrom BM, et al. Proteomics. Tissue-based map of the human proteome. *Science*. 2015;347(6220):1260419.

63. Werz O, Gerstmeier J, Libreros S, et al. Human macrophages differentially produce specific resolvin or leukotriene signals that depend on bacterial pathogenicity. *Nat Commun*. 2018;9(1):59.

64. Meng J, Moriyama M, Feld M, et al. New mechanism underlying IL-31-induced atopic dermatitis. *J Allergy Clin Immunol*. 2018;141(5):1677-1689 e1678.

65. Taira BR, Singer AJ, McClain SA, Zimmerman T. The effects of brain natriuretic peptide on scar formation in incisional rat wounds. *Acad Emerg Med*. 2008;15(10):945-948.

66. Kiguchi N, Sukhtankar DD, Ding H, et al. Spinal functions of B-type natriuretic peptide, gastrin-releasing peptide, and their cognate receptors for regulating itch in mice. *J Pharmacol Exp Ther*. 2016;356(3):596-603.

67. Solinski HJ, Kriegbaum MC, Tseng P-Y, et al. Nppb neurons are sensors of mast cell-induced itch. *Cell Rep*. 2019;26(13):3561-3573 e3564.

68. Li ZW, Wu B, Ye P, Tan ZY, Ji YH. Brain natriuretic peptide suppresses pain induced by BmK I, a sodium channel-specific modulator, in rats. *J Headache Pain*. 2016;17(1):90.

69. Zhang F-X, Liu X-J, Gong L-Q, et al. Inhibition of inflammatory pain by activating B-type natriuretic peptide signal pathway in nociceptive sensory neurons. *J Neurosci*. 2010;30(32):10927-10938.

70. Goswami SC, Thierry-Mieg D, Thierry-Mieg J, et al. Itch-associated peptides: RNA-Seq and bioinformatic analysis of natriuretic precursor peptide B and gastrin releasing peptide in dorsal root and trigeminal ganglia, and the spinal cord. *Mol Pain*. 2014;10:44.

71. Meng J, Chen W, Wang J. Interventions in the B-type natriuretic peptide signalling pathway as a means of controlling chronic itch. *Br J Pharmacol.* 2020;177(5):1025-1040.

72. Kuhn M. Endothelial actions of atrial and B-type natriuretic peptides. *Br J Pharmacol.* 2012;166(2):522-531.

73. Seomun Y, Kim JT, Joo CK. MMP-14 mediated MMP-9 expression is involved in TGF-beta1-induced keratinocyte migration. *J Cell Biochem.* 2008;104(3):934-941.

74. Li NA, Rignault-Clerc S, Bielmann C, et al. Increasing heart vascularisation after myocardial infarction using brain natriuretic peptide stimulation of endothelial and WT1(+) epicardial cells. *eLife.* 2020;9:e61050.

75. Newbern J, Birchmeier C. Nrg1/ErbB signaling networks in Schwann cell development and myelination. *Semin Cell Dev Biol.* 2010;21(9):922-928.

76. Visse R, Nagase H. Matrix metalloproteinases and tissue inhibitors of metalloproteinases: structure, function, and biochemistry. *Circ Res.* 2003;92(8):827-839.

77. Cho H, Balaji S, Hone NL, et al. Diabetic wound healing in a MMP9-/- mouse model. *Wound Repair Regen.* 2016;24(5):829-840.

78. Wysocki AB, Staiano-Coico L, Grinnell F. Wound fluid from chronic leg ulcers contains elevated levels of metalloproteinases MMP-2 and MMP-9. *J Invest Dermatol.* 1993;101(1):64-68.

79. Shapiro SD, Kobayashi DK, Ley TJ. Cloning and characterization of a unique elastolytic metalloproteinase produced by human alveolar macrophages. *J Biol Chem.* 1993;268(32):23824-23829.

80. Shipley JM, Wesselschmidt RL, Kobayashi DK, Ley TJ, Shapiro SD. Metalloelastase is required for macrophage-mediated proteolysis and matrix invasion in mice. *Proc Natl Acad Sci U S A.* 1996;93(9):3942-3946.

81. Hattori N, Mochizuki S, Kishi K, et al. MMP-13 plays a role in keratinocyte migration, angiogenesis, and contraction in mouse skin wound healing. *Am J Pathol.* 2009;175(2):533-546.

82. Layne MD, Yet S-F, Maemura K, et al. Impaired abdominal wall development and deficient wound healing in mice lacking aortic carboxypeptidase-like protein. *Mol Cell Biol.* 2001;21(15):5256-5261.

83. Ishida Y, Kuninaka Y, Nosaka M, et al. Immunohistochemical analysis on MMP-2 and MMP-9 for wound age determination. *Int J Legal Med.* 2015;129(5):1043-1048.

84. Kanno E, Tanno H, Masaki A, et al. Defect of interferon gamma leads to impaired wound healing through prolonged neutrophilic inflammatory response and enhanced MMP-2 activation. *Int J Mol Sci.* 2019;20(22):5657.

85. Yamane T, Konno R, Iwatsuki K, Oishi Y. Negative effects of a low-quality protein diet on wound healing via modulation of the MMP2 activity in rats. *Amino Acids.* 2020;52(4):505-510.

86. Cook H, Stephens P, Davies KJ, Thomas DW, Harding KG. Defective extracellular matrix reorganization by chronic wound fibroblasts is associated with alterations in TIMP-1, TIMP-2, and MMP-2 activity. *J Invest Dermatol.* 2000;115(2):225-233.

87. Iadarola MJ, Panula P, Majane EA, Yang YT. The opioid octapeptide Met5-enkephalin-Arg6-Gly7-Leu8: characterization and distribution in rat spinal cord. *Brain Res.* 1985;330(1):127-134.

88. Majane EA, Iadarola MJ, Yang HY. Distribution of Met5-enkephalin-Arg6, Phe7 in rat spinal cord. *Brain Res.* 1983;264(2):336-339.

89. Noda M, Furutani Y, Takahashi H, et al. Cloning and sequence analysis of cDNA for bovine adrenal preproenkephalin. *Nature.* 1982;295(5846):202-206.

90. Sapio MR, Iadarola MJ, Loydpierson AJ, et al. Dynorphin and enkephalin opioid peptides and transcripts in spinal cord and dorsal root ganglion during peripheral inflammatory hyperalgesia and allodynia. *J Pain.* 2020;21(9-10):988-1004.

91. Slominski AT, Zmijewski MA, Zbytek B, et al. Regulated proenkephalin expression in human skin and cultured skin cells. *J Invest Dermatol.* 2011;131(3):613-622.

92. Shime H, Odanaka M, Tsuiji M, et al. Proenkephalin(+) regulatory T cells expanded by ultraviolet B exposure maintain skin homeostasis with a healing function. *Proc Natl Acad Sci U S A.* 2020;117(34):20696-20705.

93. Moehring F, Cowie AM, Menzel AD, et al. Keratinocytes mediate innocuous and noxious touch via ATP-P2X4 signaling. *Elife.* 2018;7:e31684.

94. Moehring F, Halder P, Seal RP, Stucky CL. Uncovering the cells and circuits of touch in normal and pathological settings. *Neuron.* 2018;100(2):349-360.

95. Raziyeva K, Kim Y, Zharkinbekov Z, Kassymbek K, Jimi S, Saparov A. Immunology of acute and chronic wound healing. *Biomolecules.* 2021;11(5):700.

96. Kroin JS, Buvanendran A, Nagalla SK, Tuman KJ. Postoperative pain and analgesic responses are similar in male and female Sprague-Dawley rats. *Can J Anaesth.* 2003;50(9):904-908.

97. Gubbels Bupp MR. Sex, the aging immune system, and chronic disease. *Cell Immunol.* 2015;294(2):102-110.

98. Rosen S, Ham B, Mogil JS. Sex differences in neuroimmunity and pain. *J Neurosci Res.* 2017;95(1–2):500-508.

SUPPORTING INFORMATION

Additional Supporting Information may be found online in the Supporting Information section.